Transportation Geotechnics 55 (2025) 101715

Contents lists available at ScienceDirect

Transportation Geotechnics

journal homepage: www.elsevier.com/locate/trgeo

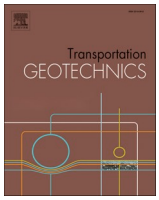

Original Article

Probabilistic simulation of TSD-based pavement deflections for Bayesian updating of material parameters

Ze Zhou Wang [a], Zhaojie Sun [a,*], Bachar Hakim [b], Buddhima Indraratna [c], Abir Al-Tabbaa [d]

[a] Marie Skłodowska-Curie Fellow, Department of Engineering, University of Cambridge, Cambridge CB3 0FA, United Kingdom
[b] Director of Roads Asset Management, AECOM Ltd, United Kingdom
[c] School of Civil and Environmental Engineering, University of Technology Sydney, Australia
[d] Department of Engineering, University of Cambridge, Cambridge CB3 0FA, United Kingdom

ARTICLE INFO

Keywords:
Bayesian model updating
Parameter inference
Traffic speed deflectometer
Numerical model
Machine learning
Probabilistic analysis

ABSTRACT

Compared to the Falling Weight Deflectometer (FWD) technology, Traffic Speed Deflectometer (TSD) provides continuous, non-destructive monitoring of pavement structural health. This feature has prompted many authorities worldwide to explore its potential in network-level pavement structural evaluation. Through parameter inference using TSD measurements, engineers can obtain physics-based evidence regarding pavement material parameters, which is crucial for informed decision-making on road operations and maintenance. However, three key challenges in existing TSD-based parameter inference have limited its practical uptake: (i) many studies introduce an intermediate correlation between TSD data and FWD data for FWD-based parameter inference, which adds extra uncertainty; (ii) conventional deterministic inference workflows yield estimates without uncertainty quantification; and (iii) high–fidelity simulations incur prohibitive computational costs, limiting real-time or near-real-time parameter inference. To overcome these gaps, this study presents a methodological framework for probabilistic parameter inference using TSD measurements. The innovation lies in the synergistic combination of: (i) a physics-based simulator, PaveMove, that directly simulates pavement responses under TSD dynamic loading, (ii) machine learning surrogates to accelerate PaveMove calculations, and (iii) Bayesian updating to transform traditional deterministic parameter inference into a probabilistic framework that explicitly incorporates multiple material and measurement uncertainties. The proposed framework is rigorously validated and compared with conventional parameter inference techniques. The results indicate that the proposed framework effectively addresses the limitations inherent in traditional techniques and provides more accurate, consistent, and reliable results of parameter inference. The proposed framework paves the way for the broader adoption of TSD technology in practice, ultimately permitting real-time, uncertainty-aware pavement management at the network scale.

Introduction

Road infrastructure is a fundamental component of modern society [1,2,3,4]. However, pavements, as critical components of road infrastructure, are susceptible to deterioration due to a combination of factors, including repeated traffic loading, environmental conditions [5,6], material aging [7,8], and inadequate maintenance. The resulting poor road conditions can be substantial and lead to reduced ride quality, safety hazards, increased vehicle operating costs [9], and higher maintenance expenses, among other issues. Therefore, accurate measurement and prediction of pavement performance are crucial for implementing timely and cost-effective pavement maintenance and rehabilitation strategies.

Various methods have been developed to assess and predict pavement performance. Data-driven methods have gained considerable attention in recent years [10,11,12,13]. However, data-driven approaches are heavily reliant on the availability of large, high-quality datasets, which can be challenging and costly to obtain. Furthermore, machine learning models are often criticized for their "black box" nature, where the underlying mechanisms driving the predictions may not be fully transparent [14,15,16]. As an alternative, field tests and sensor-based field measurements have been employed in pavement

* Corresponding author.
E-mail addresses: zw437@cam.ac.uk, wangzz@u.nus.edu (Z.Z. Wang), zs442@cam.ac.uk (Z. Sun), bachar.hakim@aecom.com (B. Hakim), buddhima.indraratna@uts.edu.au (B. Indraratna), aa22@cam.ac.uk (A. Al-Tabbaa).

https://doi.org/10.1016/j.trgeo.2025.101715
Received 11 June 2025; Received in revised form 27 August 2025; Accepted 7 September 2025
Available online 8 September 2025

performance evaluation [17,18,19,20]. These methods provide direct measurements of pavement responses and often offer valuable insights into structural behavior. However, the installation and maintenance of sensors can be complex and expensive, and they typically provide only localized measurements.

In this context, non-embedded sensors offer additional approaches for pavement performance evaluation. The Falling Weight Deflectometer (FWD) [21,22,23] is a widely used non-destructive testing (NDT) device. However, FWD is a stationary test method that necessitates traffic management, which can be time-consuming and disruptive. As a result, the Traffic Speed Deflectometer (TSD), a more recent NDT technology, has been developed to measure pavement responses under moving traffic loads [20,24,25,26,27].

TSD offers the distinct advantage of efficient, network-level pavement evaluation without disrupting traffic flow. It measures deflection velocity (slope) at traffic speed using Doppler lasers and calculates corresponding pavement deflections. Multiple techniques have been proposed for this task, including some advanced ones [28,29]. Studies have shown that pavement modulus back-calculated from TSD measurements correlate well with those from FWD measurements [15,16,30]. Due to its mobile nature, TSD is more applicable for evaluating pavement conditions and structural capacities at the network level, in contrast to FWD, which is primarily used for project-level assessment. However, research on TSD is still relatively limited and less established compared to FWD-based prediction models [37]. This highlights the need for new models specifically tailored to TSD measurements. Katicha et al. [25] provided a comprehensive review of TSD research and applications in the United States over the past decade.

In many cases, sensor and field test data require interpretation to obtain meaningful information about pavement structural conditions. Parameter inference, also known as parameter identification, back-analysis, or back-calculation, is a commonly used approach [22,24,31,32,33,34]. This process involves using measured pavement responses to estimate key pavement parameters, such as layer modulus and thicknesses, which are crucial for pavement structural analysis and performance prediction. Parameter identification typically comprises several components. First, a model is needed to simulate pavement responses under loading. Various methods can be used, including analytical solutions, finite element method (FEM) [35], spectral element method [36], and semi-analytical methods. Second, an algorithm is required to estimate pavement parameters by evaluating the discrepancies between measured and simulated pavement responses. These algorithms can be broadly classified into deterministic and probabilistic approaches. Deterministic approaches, such as residual minimization [32,33], aim to identify the single “best-fit” set of parameters by minimizing the difference between measured and simulated pavement responses. In contrast, probabilistic approaches, such as Bayesian updating, provide a framework for quantifying the uncertainties associated with the parameter estimates.

Motivated by these needs, the present study pioneers the investigation of probabilistic parameter inference using TSD measurements. However, three key challenges in existing TSD-based parameter inference have limited its practical adoption:

- First, many existing strategies begin by correlating TSD data with FWD data before using FWD-based techniques for parameter inference [24]. This is likely due to the limited availability of methods capable of simulating pavement responses under TSD loading, as well as the long-standing industry reliance on FWD in pavement management. However, Hamidi et al. [37] highlighted that the conversion between TSD and FWD data is not universally applicable and depends on numerous factors. As a result, such conversions inevitably introduce uncertainties, which may hinder the accuracy and reliability of parameter inference.
- Second, parameter identification coupled with high-fidelity numerical simulations can be computationally demanding due to the iterative nature of the process. For example, Liu et al. [38] reported that each simulation using ABAQUS requires about 420 s, and even with improved techniques, the runtime remained around 120 s. While this may be acceptable for interpreting FWD measurements, it is incompatible with the continuous nature of TSD data collection, which is expected to yield real-time or near-real-time interpretations. The broader application of TSD is hindered by this limitation.
- Third, the presence of uncertainties poses a significant challenge. Material properties are inherently variable. Uncertainties also arise from modelling assumptions and field measurements. Conventional deterministic parameter inference techniques often struggle to adequately account for these sources of uncertainty, which can then limit their reliability and robustness [22,37].

Given these limitations and challenges, there is a need for robust and efficient approaches for probabilistic pavement structural evaluation. This study addresses this need by presenting a novel framework for the probabilistic interpretation of TSD measurements. The innovation lies in the synergistic combination of three core components, each specifically designed to tackle the challenges outlined above:

- First, a physics-based simulator, PaveMove, was developed to directly simulate pavement responses under TSD dynamic loading. The use of this model eliminates the common intermediate step of correlating TSD measurements with FWD measurements for parameter inference.
- Second, to address the high computational demand associated with repeated high-fidelity simulations in parameter inference, machine learning was employed to develop surrogate models that enable rapid computation without compromising accuracy.
- Third, Bayesian updating was incorporated to transform conventional deterministic parameter inference into a fully probabilistic framework. Multiple material and measurement uncertainties can then be explicitly considered in parameter inference.

In the present study, the proposed framework was rigorously validated using simulated TSD measurements. A comparison with conventional parameter inference techniques was also conducted. The results indicate that the proposed framework effectively addresses the limitations inherent in traditional techniques and provides more accurate, consistent, and reliable parameter estimates. This framework paves the way for the broader adoption of TSD technology, ultimately permitting real-time, network-scale pavement management that explicitly accounts for uncertainty.

Key Components in the Probabilistic Framework

PaveMove

A software developed in-house called PaveMove is used to simulate pavement responses under TSD dynamic loading. In PaveMove, pavement is modelled as a layered structure with TSD loading represented as a moving surface load, as shown in Fig. 1. The simulation of pavement responses under a moving TSD loading is based on a Spectral Element Method (SEM) procedure, which comprises the following steps [39]:

(i) The moving load problem is transformed into a coordinate system that travels with the load.
(ii) The problem is further transformed to the wavenumber-frequency domain via a forward Fourier transform. The stiffness matrices for both a layer spectral element and a semi-infinite spectral element can then be derived.
(iii) The global stiffness matrix for the pavement structure is assembled, and appropriate boundary conditions are applied to compute the nodal responses.

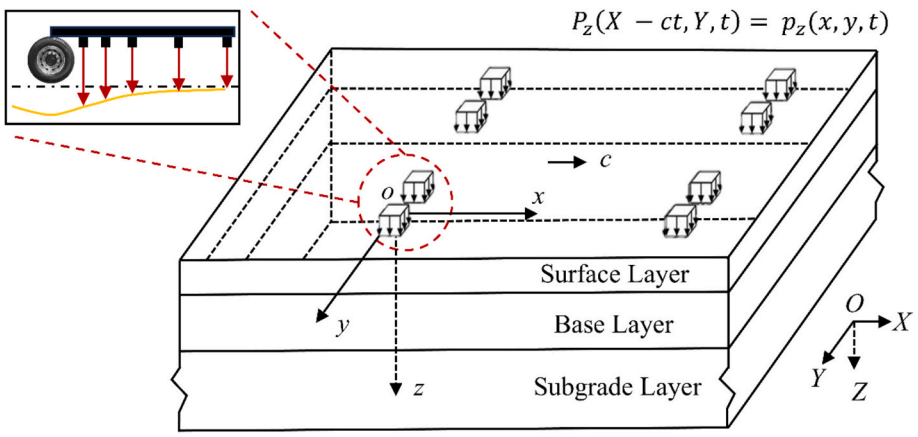

Fig. 1. A typical pavement system and TSD configuration simulated in PaveMove.

(iv) The calculated response fields within the pavement layers are converted back to the space–time domain using an inverse Fourier transform.
(v) If necessary, the response fields in the moving coordinate system are transformed back to the stationary coordinate system.

The SEM approach combines the geometric flexibility of the Finite Element Method (FEM) with the high accuracy characteristics of spectral methods. For pavement dynamic analysis, each pavement layer is modelled by a single spectral element with accurate response formulations. This strategy minimizes the number of elements required, which is equal to the number of pavement layers, and reduces the size of the global stiffness matrix, further improving computational efficiency. In addition, the use of precise shape functions further enhances the accuracy of the results. As a result, the SEM-based procedure in PaveMove can accurately and efficiently predict pavement responses under moving TSD loadings. In PaveMove, users can define the number of pavement layers, specify the material parameters of each layer, set the speed of the TSD device, and configure the TSD loading conditions. Additionally, each pavement layer can be simulated as purely elastic, elastic with hysteretic damping, or viscoelastic, which enables a versatile approach to pavement modelling under various dynamic conditions and material constitutive behavior.

The accuracy of PaveMove has been rigorously validated. First, its numerical performance under purely elastic conditions was compared with the simulation results presented in Nielsen [40], which used a semi-analytical method and elastic materials. The agreement shown in Fig. 2(a) confirms the numerical accuracy of PaveMove. Furthermore, real-world TSD measurements from Nielsen [40] were used to validate PaveMove further, with the results shown in Fig. 2(b). For both validations, the parameter values reported in Nielsen [40] were used as the inputs for PaveMove. The ability of PaveMove to simulate damping material behaviour allows it to accurately replicate both the magnitude and shape of the deflection slope observed in field TSD results. These validations underscore the robust accuracy of PaveMove in practical applications.

Bayesian model updating

Bayesian updating is an effective probabilistic technique used to infer statistical information about single or multiple material parameters using field measurements. This is achieved through the estimation of the posterior probability density function (PDF) of these material parameters [41]. According to the Bayes' theorem, the posterior PDF is calculated as follows:

$$f_X(\boldsymbol{x}|\widehat{\boldsymbol{y}}) = k_1 \bullet f_X(\boldsymbol{x}) \bullet L(\widehat{\boldsymbol{y}}) \tag{1}$$

where $f_X(\boldsymbol{x})$ and $f_X(\boldsymbol{x}|\widehat{\boldsymbol{y}})$ represent, respectively, the prior and posterior PDFs of material parameters $\boldsymbol{X}$, $\boldsymbol{X} = (X_1, X_2, X_3, \ldots, X_n)$, with n being the number of material parameters to be updated using field measurements $\widehat{\boldsymbol{y}}$, $\widehat{\boldsymbol{y}} = (\widehat{y_1}, \widehat{y_2}, \widehat{y_3}, \ldots, \widehat{y_m})$, where m is the number of field measurements; $\boldsymbol{x}$ is a sample of $\boldsymbol{X}$. k_1 is a normalization constant that ensures the integral of $f_X(\boldsymbol{x}|\widehat{\boldsymbol{y}})$ over the probabilistic domain of $\boldsymbol{X}$ is equal to 1, i.e., $k_1 = 1/\int f_X(\boldsymbol{x}) \bullet L(\widehat{\boldsymbol{y}}) d\boldsymbol{x}$; and $L(\widehat{\boldsymbol{y}})$ is the likelihood function.

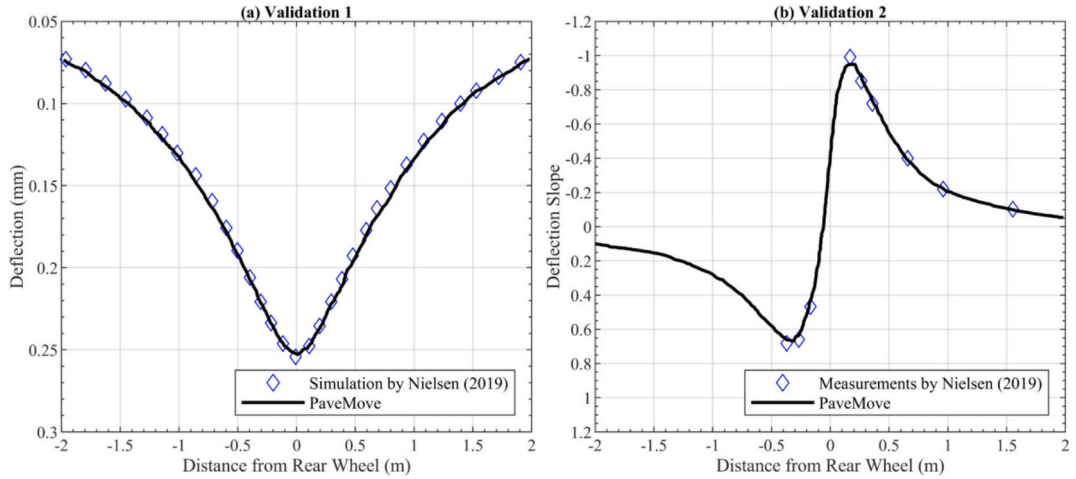

Fig. 2. Validation of PaveMove.

In addition, to fully utilize field measurements to update the probability distributions of material parameters, it is necessary to first construct the likelihood function based on the various types of field information. This is a crucial step in Bayesian model updating [42]. Conceptually, the likelihood function represents the probability of the occurrence of the field information $\hat{\boldsymbol{y}}$ given that the uncertain parameters $\boldsymbol{X}$ take on a specific value $\boldsymbol{x}$. Mathematically, it is expressed as follows:

$$L(\hat{\boldsymbol{y}}) \propto f(\hat{\boldsymbol{y}}|\boldsymbol{X}=\boldsymbol{x}) \tag{2}$$

In practice, due to limitations in the precision of instruments and experimental apparatus, human errors, or other random factors, measurement errors are unavoidable. Therefore, measurement errors are typically treated as additional uncertainties that can be incorporated into the simulated responses of the system under study. Similarly, model error exists in any simulation model due to oversimplifications of real-world conditions in engineering systems, such as boundary conditions and constitutive models of the materials. Because of model error, the responses of an engineering system evaluated by a model generally do not perfectly align with the observed performance of the system. Similar to measurement errors, model errors can be added to the simulated responses of the engineering system under study. In many cases, measurement and model errors are assumed to follow a normal distribution (e.g., [4,42,43]) with a mean of zero and a standard deviation of $\boldsymbol{\sigma}_U$. In other instances, biases might be considered, leading to measurement and model errors having a non-zero mean of $\boldsymbol{\mu}_U$. Due to the presence of these errors, assuming a normal distribution, the corresponding likelihood function can be constructed as follows:

$$L(\hat{y}_i) = \frac{1}{\sqrt{2\pi}\sigma_{i,U}} e^{\left[-\frac{1}{2\sigma_{i,U}^2}\left(\hat{y}_i - g_{i,X}(\boldsymbol{x}) - \mu_{i,U}\right)^2\right]} \tag{3}$$

where $\hat{y}_i$ is the i-th field measurement; $g_{i,X}(\boldsymbol{x})$ is the simulated system response at the i-th field measurement location using the parameter sample $\boldsymbol{x}$; $\mu_{i,U}$ and $\sigma_{i,U}$ are, respectively, the mean and standard deviation of the uncertainty at the i-th measurement location. The equation above illustrates the construction of the likelihood function using a single field measurement and assuming normally distributed uncertainties.

When multiple field measurements are used simultaneously for parameter inference, a correlation matrix $\boldsymbol{C}$, which describes the dependency of uncertainties at these multiple measurement locations, is needed to construct the joint normal probability distribution as follows:

$$L(\hat{\boldsymbol{y}}) = \frac{1}{2\pi^{\frac{m}{2}}|\boldsymbol{C}|^{\frac{1}{2}}} e^{\left[-\frac{1}{2}(\hat{\boldsymbol{y}} - g_X(\boldsymbol{x}) - \boldsymbol{\mu}_U)^T \boldsymbol{C}^{-1} (\hat{\boldsymbol{y}} - g_X(\boldsymbol{x}) - \boldsymbol{\mu}_U)\right]} \tag{4}$$

where $|\boldsymbol{C}|$ is the determinant of $\boldsymbol{C}$.

In practice, the choice of the correlation matrix can vary depending on the type of field measurement. For measurements taken from separate sensors, such as a group of strain gauges, it is commonly assumed that the uncertainties associated with these measurements are independent. However, when multiple measurements are taken by a single sensor, such as an inclinometer, measurement uncertainties are typically correlated [3,4]. Similarly, modelling uncertainties arising from the assumptions or simplifications inherent in the numerical model are also typically correlated [44]. However, it is often challenging to obtain precise correlation values, so the assumption of independence is frequently employed.

In many instances, it is not feasible to calculate the posterior distributions analytically. Therefore, sampling techniques are often employed in Bayesian updating. The Markov chain Monte Carlo simulation using the Metropolis-Hastings algorithm (MCMC-MH) is a common technique for this task, and further details can be found in [22,44]. It is important to note that the initial samples generated by the algorithm may not accurately represent the posterior PDF because the Markov chain has not reached a steady state. Therefore, in practice, a certain number of initial samples are often considered as burn-in samples and are discarded from the final posterior samples. In addition, the scale factor in the MCMC-MH algorithm often needs fine-tuning through a trial-and-error process to ensure the accuracy and efficiency of the results.

Machine learning as surrogates

As previously emphasized, parameter inference coupled with numerical simulations can be a computationally intensive process. For example, the MCMC-MH algorithm may necessitate several thousand samples to adequately approximate the posterior distribution. Similarly, conventional deterministic parameter inference techniques may also require a few hundred samples for the optimization algorithm to converge to an optimal solution. Therefore, a surrogate model is often employed to expedite these calculations while still effectively representing the underlying physics of the simulation models.

The fundamental principle of surrogate modelling involves approximating the complex physics-based relationship between numerically calculated system responses and their corresponding input parameters using a simpler function, and this is often achieved through training a machine learning model using data generated from the original simulation model. Once the surrogate model has been adequately trained and tested, it can be used as a substitute for the original simulation model, permitting rapid calculations with significantly reduced computational resources. In the present study, surrogate modelling is specifically employed to predict pavement deflections under TSD dynamic loadings based on a defined set of input parameters.

The surrogate model is specifically designed for the typical three-layer pavement system illustrated in Fig. 1. Table 1 provides a comprehensive summary of all the input parameters considered in the development of this global surrogate model. While certain parameters

Table 1
Input parameter space for surrogate modelling.

Parameters		Lower Bound	Upper Bound	Remarks
Surface layer	Modulus, $E_{surface}$ (MPa)	100	30,000	[25,45,46,47,48,49,50,51]
	Damping ratio, $\varepsilon_{surface}$	0.01	0.3	
	Poisson's ratio, $\nu_{surface}$	0.25	0.35	
	Unit weight, $\gamma_{surface}$ (kN/m^3)	22	25	
	Thickness, $h_{surface}$ (m)	0.05	0.5	
Base layer	Modulus, E_{base} (MPa)	50	30,000	
	Damping ratio, ε_{base}	0.01	0.2	
	Poisson's ratio, ν_{base}	0.25	0.35	
	Unit weight, γ_{base} (kN/m^3)	18	22	
	Thickness, h_{base} (m)	0.1	0.7	
Subgrade layer	Modulus, $E_{subgrade}$ (MPa)	10	500	
	Damping ratio, $\varepsilon_{subgrade}$	0.01	0.1	
	Poisson's ratio, $\nu_{subgrade}$	0.25	0.35	
	Unit weight, $\gamma_{subgrade}$ (kN/m^3)	16	20	
Truck	Truck speed (km/h)	50	100	
	Axle load (kN)	40	130	

may have a less significant impact compared to the modulus and thickness of the three layers, they are included to ensure the surrogate model's applicability as a general global model. Based on a thorough review of existing literature (i.e., refer to Table 1), the conservative upper and lower bounds of all parameters are also detailed in the table. The surrogate model will be trained to accurately represent the entire parameter space. It is worth highlighting that these bounds have been intentionally broadened beyond typical values reported in the literature to ensure the surrogate model can handle unusual or extreme scenarios. The outputs of the model consist of the pavement deflection measured at 0.25 m intervals, ranging from 1.5 m behind the measuring wheel to 5 m ahead of it. The subsequent steps outline the construction of this surrogate model:

(i) Based on the defined bounds summarized in Table 1, Latin Hypercube sampling is utilized to generate 25,000 parameter combinations.
(ii) PaveMove is employed to simulate each of these 25,000 parameter combinations. The resulting pavement deflections at the multiple measurement locations are extracted.
(iii) The generated dataset, consisting of 25,000 input samples each with 16 parameters and corresponding 25,000 output samples each with 27 deflection measurements, is partitioned into a training dataset (70 %) and a validation dataset (30 %) for training an Artificial Neural Network (ANN) model.
(iv) Based on the parameter information in Table 1, an additional 5,000 parameter combinations that are different from the initial 25,000 samples are further generated. These combinations are simulated using PaveMove to provide an independent test dataset for an unbiased evaluation of the predictive performance of the trained global surrogate model.
(v) After training and validating the global surrogate model using this unseen data, it can be confidently used as a computationally efficient alternative to the original PaveMove model for subsequent bulk calculations.

The architecture and hyperparameters of the ANN model are summarized in Table 2. Since ANN is an established machine learning model, detailed technical descriptions are omitted in the present study. Fig. 3 presents the key results evaluating the performance of the trained ANN model. Fig. 3(a) illustrates the training and validation losses, which are terminated after approximately 1,000 epochs due to the early stopping criteria specified in Table 2. This is an important configuration that minimizes overfitting and preserves the generalization capability of the model. Fig. 3(b) compares the PaveMove-predicted pavement deflection profile with the ANN-predicted results for a case randomly selected from the 5,000 test samples. The remarkable match between the ANN and PaveMove outputs highlights the ANN's strong predictive performance, even for previously unseen input data. To further validate the model, Fig. 3(c) compares the ANN-predicted and PaveMove-predicted deflections for all 5,000 test samples, resulting in a total of 135,000 data points (27 deflection points per sample). The high coefficient of determination (i.e., $r^2 > 0.99$) confirms the ANN's robust accuracy across the entire test dataset. In addition, the individual r^2 values for each of the 27 measurement locations, shown in Fig. 3(d), indicate consistently high prediction accuracy across the spatial deflection profile. This level of performance is justifiable given that the ANN model is trained on data generated by a numerical simulator grounded in well-defined physical laws.

Table 2
Configurations of the ANN model.

Hyper-parameters	Setting
Number of hidden layer	3
Number of neurons in each hidden layer	10
Training algorithm	Bayesian regularization back-propagation
Maximum iteration	20,000
Early stop criterion	500
Loss function	Sum squared errors

The trained ANN model is employed in the subsequent Bayesian updating using simulated TSD measurements. While simulating 1,000 samples using the original PaveMove simulator requires approximately 25 h, the trained ANN model can complete the same task within a second. This substantial improvement in computational efficiency enables real-time or near-real-time parameter inference. In addition, although TSD trucks do not directly measure deflection, the current study focuses on deflection itself, which serves as a more intuitive and interpretable response variable. In practice, there are several established techniques to convert deflection slope to deflection, and the surrogate modelling framework developed here can be readily extended to work with deflection slope as well.

Probabilistic Simulation of TSD for Sensitivity Analysis

Implementation procedures

Probabilistic sensitivity analyses are first conducted to evaluate the influence of uncertainties in pavement material parameters on pavement deflections. The trained ANN model is used as the forward simulator for this purpose. A key advantage of probabilistic sensitivity analysis lies in its ability to explicitly account for uncertainties in material parameters and permit the computation of both the mean and standard deviation of pavement deflections. This provides a more comprehensive understanding of how different parameters affect pavement responses. In contrast, conventional deterministic sensitivity analysis only yields single-value predictions and does not capture the uncertainty associated with the results.

Fig. 4 illustrates an example of probabilistic simulation of pavement deflections under TSD dynamic loading using the typical parameter statistics listed in Table 3. A total of 5,000 parameter combinations are generated using Monte Carlo sampling based on the statistics. The three uncertain modulus parameters are assumed to follow a lognormal distribution, while all other uncertain parameters follow a normal distribution. All distributions are truncated at the upper and lower bounds defined in Table 1. The trained ANN model is then used to simulate all 5,000 parameter combinations within two seconds. Each grey line shown in Fig. 4(a) represents the deflection profile for an individual Monte Carlo sample, while the mean deflection profile is also plotted for reference. Fig. 4(b) shows the statistical distribution of pavement deflections at the wheel location, and both the mean and coefficient of variation (CoV) of deflections are calculated. As shown in the figure, the resulting uncertainty in deflections is significant (e.g., CoV = 18.2 %), highlighting the importance of explicitly incorporating parameter uncertainty in the simulation and interpretation of TSD measurements.

Table 4 summarizes the parametric cases considered in the present study. A total of 5 cases are examined, each focusing on the effect of uncertainty in a single parameter—the modulus of the three layers and the thickness of the surface and base layers. In each case, all other parameters are held deterministic at the mean values summarized in the table. For each case, 5,000 parameter combinations are generated using Monte Carlo sampling. Following the visualization shown in Fig. 4, selected results from Case 3 of the sensitivity analyses are presented in Fig. 5.

Fig. 5 (a) to (c) show the results of varying the CoV of $E_{subgrade}$ from 0.1 to 0.3, with a constant mean of 20 MPa and all other parameters remaining constant. Similarly, Fig. 5 (d) to (f) show the results with a higher mean $E_{subgrade}$ of 100 MPa under the same CoV variations. It is evident that both the magnitude and statistical variability of pavement deflections are strongly influenced by uncertainties in $E_{subgrade}$. To facilitate a systematic investigation of parameter sensitivity, the results are broadly categorized into two types—intra-project sensitivity and

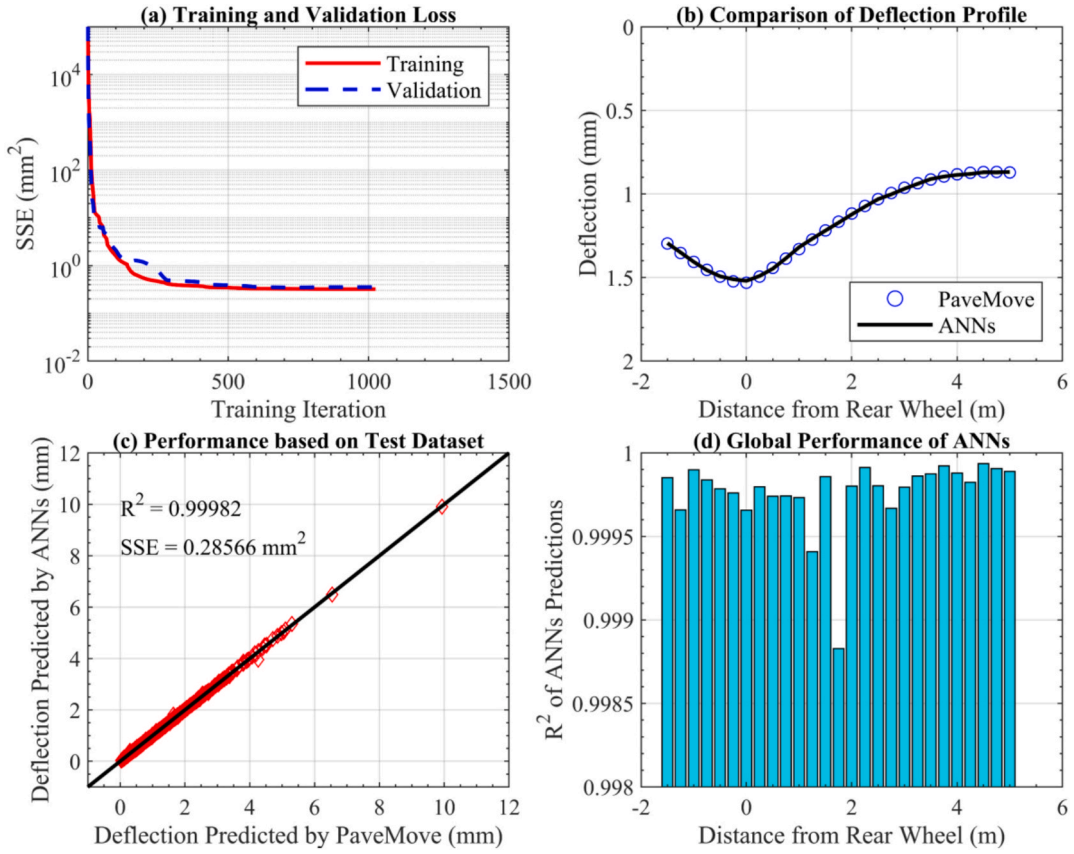

Fig. 3. Performance of the trained ANN surrogate model.

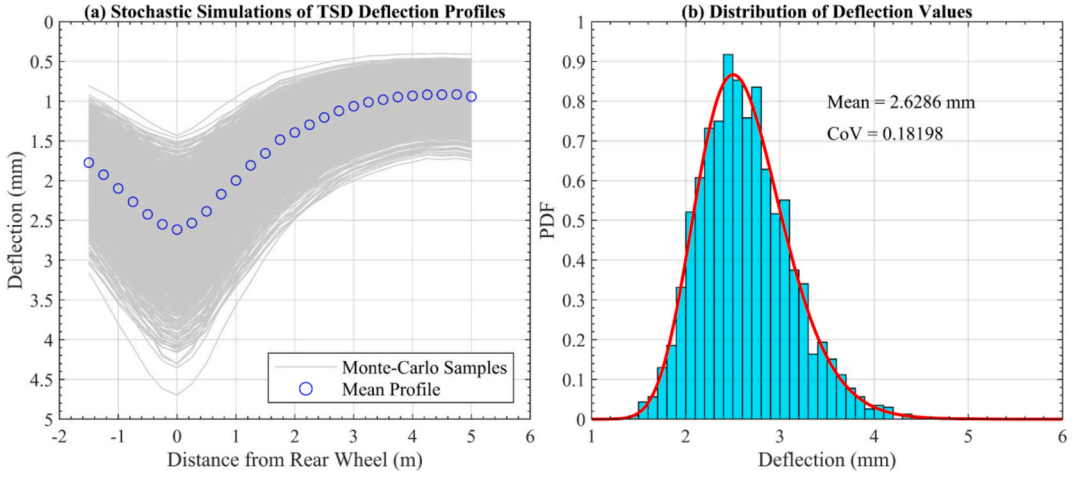

Fig. 4. An example of stochastic simulation of pavement deflection under TSD dynamic loading.

inter-project sensitivity:

- Intra-project sensitivity evaluates the effects of CoV while keeping the parameter mean fixed. This reflects a scenario within a single project, where mean material properties are generally known, but their statistical variability is uncertain. For example, the comparison across Fig. 5 (a) to (c) represents intra-project sensitivity. In this context, the CoV of the pavement deflection is the key quantity of interest.
- Inter-project sensitivity investigates the effects of varying the mean of a parameter while holding its CoV constant. This reflects comparisons across different projects where material types and designs may vary substantially. For example, comparing Fig. 5 (a) with (d) or Fig. 5 (b) with (e) highlights inter-project sensitivity. In this case, the mean pavement deflection is the main response variable of interest.

Results of sensitivity analysis

Fig. 6 shows the results of the sensitivity analyses for Case 1 (refer to Table 4), which investigates the effects of $E_{surface}$. Two subcases are considered: (i) a stiff base over a soft subgrade, and (ii) a soft base over a stiff subgrade. To simplify the discussion, only the deflection at the measuring wheel location is analyzed. For meaningful comparisons across different cases, it is essential to examine normalized values. In

Table 3
Typical statistical characteristics of material parameters for a three-layer pavement system.

Parameters		Mean	CoV
Surface	$E_{surface}$ (MPa)	3000	0.2
	$\varepsilon_{surface}$	0.1	0.15
	$\nu_{surface}$	0.3	0.1
	$\gamma_{surface}$(kN/m^3)	22.5	0.05
	$h_{surface}$ (m)	0.1	0.1
Base	E_{base} (MPa)	5000	0.2
	ε_{base}	0.1	0.1
	ν_{base}	0.3	0.1
	γ_{base}(kN/m^3)	21	0.05
	h_{base} (m)	0.3	0.15
Subgrade	$E_{subgrade}$ (MPa)	60	0.2
	$\varepsilon_{subgrade}$	0.05	0.05
	$\nu_{subgrade}$	0.3	0.05
	$\gamma_{subgrade}$(kN/m^3)	18	0.05
Truck	Truck speed (km/h)	100	–
	Axle load (kN)	130	–

this regard, for inter-project sensitivity, the x-axis represents the normalized material property (i.e., normalized with respect to the upper and lower bounds shown in Table 1). The y-axis represents the relative change in mean deflection compared to the case with the lower bound material parameter value. For intra-project sensitivity, the focus is on the CoV of the material parameter and the corresponding CoV of pavement deflection. Since both quantities are normalized parameters, direct comparisons are permitted.

Fig. 6 (a) and (c) show the mean deflections based on 5,000 stochastic simulations for various cases. The results show that pavement deflection is sensitive to variations in the mean value of $E_{surface}$, though the degree of sensitivity varies. The sensitivity is more pronounced when the surface layer is softer, and the inter-project sensitivity becomes more significant with increasing $h_{surface}$. However, as the mean $E_{surface}$ increases, the effects of $h_{surface}$ diminish, indicating reduced inter-project sensitivity. In addition, the CoV of $E_{surface}$ appears to have negligible effects on the inter-project sensitivity trends.

Fig. 6 (b) and (d) show the CoV of pavement deflections. The different lines within each thickness group correspond to cases with different mean $E_{surface}$ values. In all cases, a linear relationship is observed between the CoV of $E_{surface}$ and the CoV of deflection. For the same CoV of $E_{surface}$, thicker surface layers result in higher CoV of deflection. However, the magnitude of CoV in deflection remains low, typically within 3 % to 4 %, indicating that the statistical variability of $E_{surface}$ contributes only marginally to the variability in deflection. In addition, these observed trends in both inter-project and intra-project sensitivity are largely consistent across the two subcases, despite differences in the mechanical characteristics of the base and subgrade layers.

Fig. 7 shows the results of Case 2, which focuses on the effects of the statistics of E_{base} on deflections. Two subcases are considered: (i) a soft subgrade, and (ii) a stiff subgrade. Similar to Case 1, inter-project sensitivity analysis reveals that pavement deflections are significantly influenced by variations in mean E_{base}, with higher sensitivity in softer and thicker base layers and diminishing effects for higher mean E_{base}. Over the plausible range of E_{base}, pavement deflections can vary up to 60 %. For intra-project sensitivity, a consistent linear relationship is observed between the CoV of E_{base} and the CoV of pavement deflection in all cases, and the sensitivity is also more pronounced for thicker base layers. Although the CoV of pavement deflections remains relatively small (approximately 4 % to 6 %), it is notably higher than that observed for variations in $E_{surface}$. In general, the sensitivity trends for E_{base} mirror those observed for $E_{surface}$, but the magnitude of sensitivity of E_{base} is generally slightly greater.

Fig. 8 shows the results of Case 3 that focuses on the subgrade layer. Two subcases with different values of E_{base} are considered. As shown in Fig. 8 (a), pavement deflections are highly sensitive to variations in mean $E_{subgrade}$, with deflection magnitude changing by up to 90 % over the plausible range of $E_{subgrade}$. This level of inter-project sensitivity is substantially greater than that observed for both E_{base} and $E_{surface}$. Consistent with patterns in Figs. 6 and 7, the sensitivity to changes in mean $E_{subgrade}$ is more pronounced in softer subgrades, and the general trends remain similar across the two subcases with different E_{base}. In Fig. 8 (b), a linear relationship is again observed between the CoV of $E_{subgrade}$ and the CoV of pavement deflection, affirming the presence of intra-project sensitivity. However, a key distinction emerges: the magnitude of CoV in pavement deflection due to uncertainty in $E_{subgrade}$ is substantially higher, reaching up to 20 %. This number indicates the dominant influence of uncertain $E_{subgrade}$ on the statistical behavior of pavement deflections. Moreover, the trends are consistent across different values of E_{base}, reinforcing the critical role of the subgrade layer in governing the probabilistic response of pavement systems under TSD dynamic loading.

Fig. 9 shows the results of Case 4 on the effects of $h_{surface}$ on pavement deflections. As shown in Fig. 9 (a) and (c), variations in $h_{surface}$ can lead to pavement deflection changes of up to 50 % over the plausible range, indicating a significant degree of inter-project sensitivity. Unlike the nonlinear trend observed in Fig. 6, the degree of inter-project sensitivity associated with $h_{surface}$ is moderately linear. In addition, the sensitivity is more pronounced for stiffer surface layers, although the effects tend to converge as $E_{surface}$ increases. For example, results for

Table 4
Cases considered in the probabilistic sensitivity analysis.

Case ID / Parameter[#]	1	2	3	4	5
Mean $E_{surface}$ (GPa)	**0.5-25**	3	3	0.5; 1; 2; 8; 16	3
CoV of $E_{surface}$	**0.1-0.3**	-	-	-	-
Mean E_{base} (GPa)	0.5; 5	**0.5-25**	0.5; 5	0.5; 5	0.5; 1; 2; 8; 16
CoV of E_{base}	-	**0.1-0.3**	-	-	-
Mean $E_{subgrade}$ (GPa)	0.06; 0.2	0.06; 0.2	**0.02-0.45**	0.06; 0.2	0.06; 0.2
CoV of $E_{subgrade}$	-	-	**0.1-0.3**	-	-
Mean $h_{surface}$ (m)	0.1; 0.2; 0.3	0.1	0.1	**0.1-0.4**	0.1
CoV of $h_{surface}$	-	-	-	**0.05-0.25**	-
Mean h_{base} (m)	0.3	0.1; 0.3; 0.6	0.3	0.3	**0.1-0.6**
CoV of h_{base}	-	-	-	-	**0.05-0.25**

*Other parameters follow the mean values shown in Table 3.
[#]Modulus follows a lognormal distribution, and thickness follows a normal distribution. All distributions are truncated at the upper and lower bounds listed in Table 1.

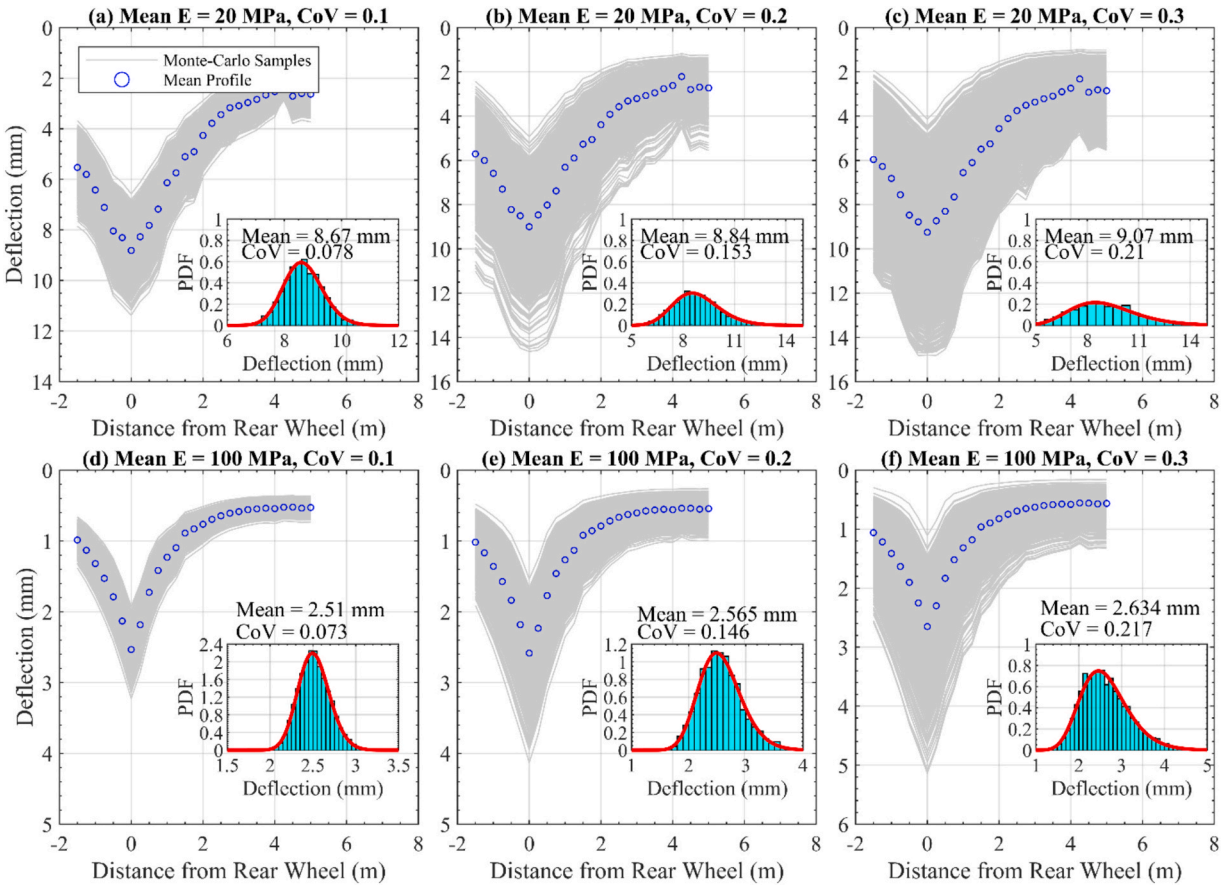

Fig. 5. Selected results of Case 3 of the probabilistic sensitivity analysis.

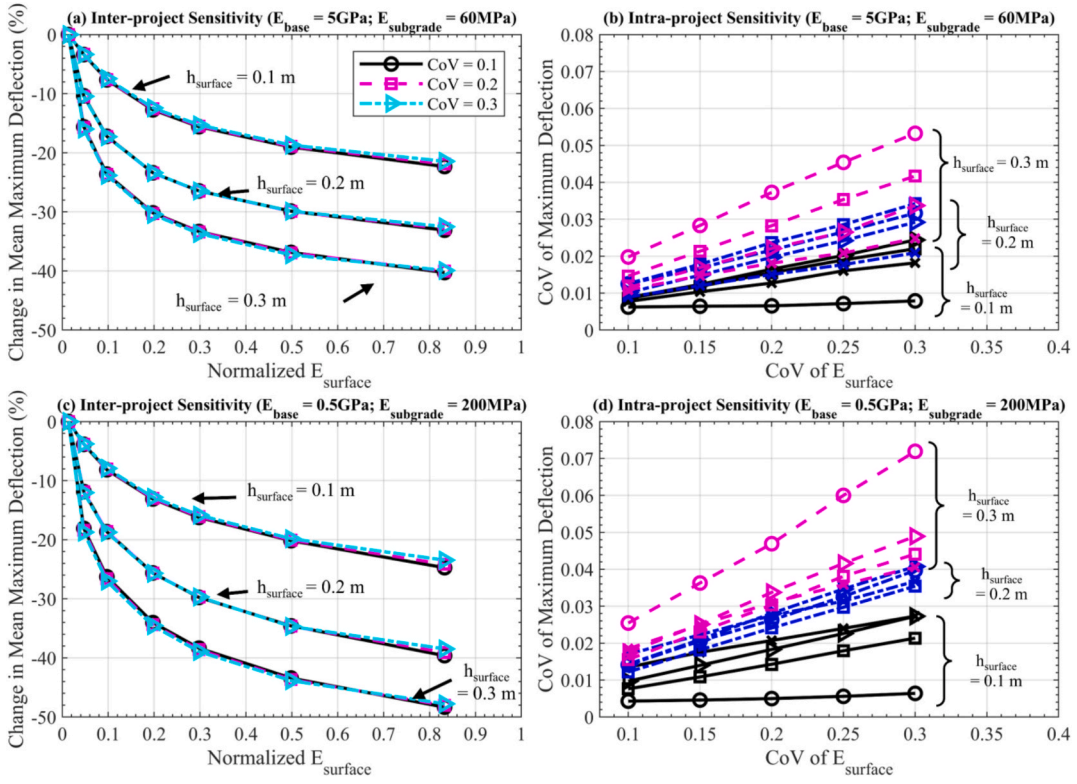

Fig. 6. Results of Case 1 of the probabilistic sensitivity analysis. The different lines shown in subplot (b) and (d) within each thickness group correspond to cases with different mean $E_{surface}$ values.

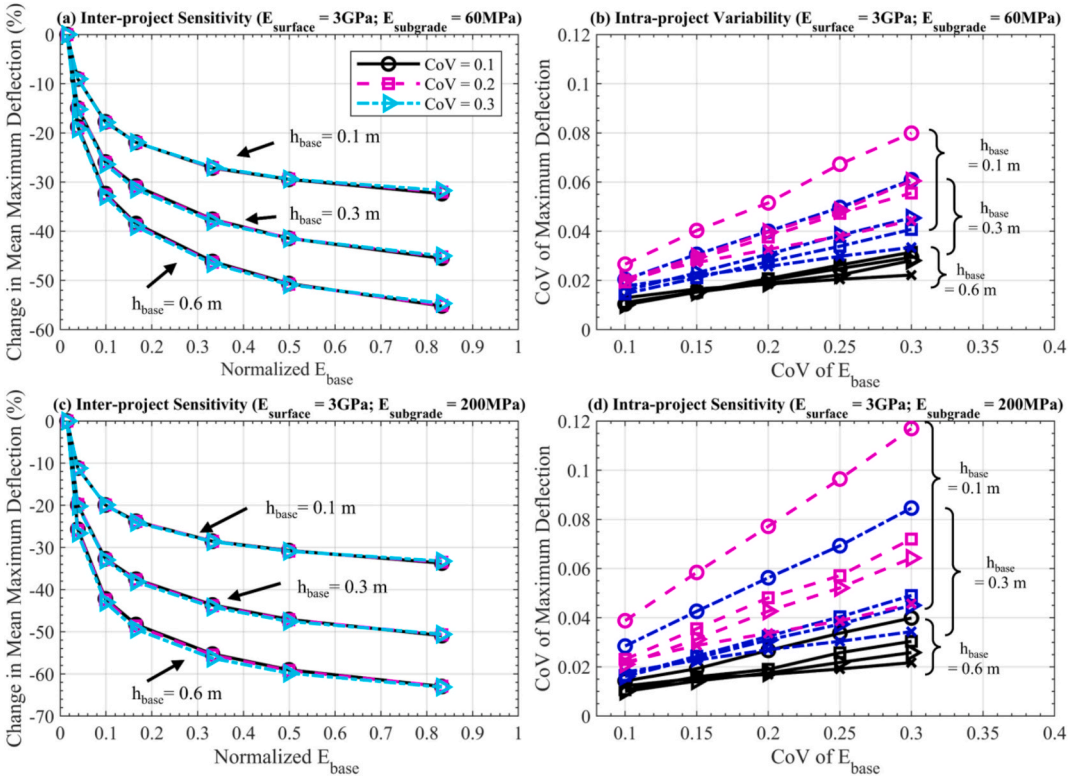

Fig. 7. Results of Case 2 of the probabilistic sensitivity analysis. The different lines shown in subplot (b) and (d) within each thickness group correspond to cases with different mean E_{base} values.

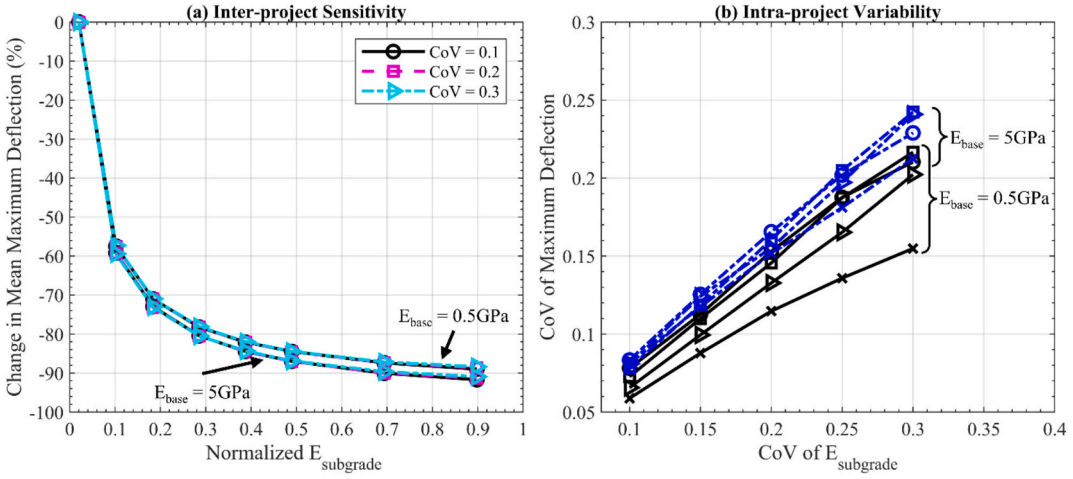

Fig. 8. Results of Case 3 of the probabilistic sensitivity analysis. The different lines shown in subplot (b) within each E_{base} group correspond to cases with different mean $E_{subgrade}$ values.

$E_{surface} = 6$ GPa and 15 GPa show only marginal differences, suggesting a diminishing influence of $h_{surface}$ at higher $E_{surface}$ values. For intra-project sensitivity, a linear relationship between the CoV of $h_{surface}$ and the CoV of deflection is also observed, as shown in Fig. 9 (b) and (d). Similar to the inter-project results, the effect of CoV of $h_{surface}$ is more noticeable for stiffer surface layers. Nevertheless, the absolute values of the CoV of deflection are still relatively small, indicating that the statistical uncertainty in $h_{surface}$ exerts only a moderate influence on the statistical variability of pavement responses.

Fig. 10 shows the results of Case 5 on the effects of h_{base}. As shown in the figure, variations in mean h_{base} result in a significant inter-project sensitivity, with deflection changes reaching up to 60 % over the plausible range. The relationship between mean h_{base} and pavement deflection is moderately linear, and the sensitivity is more pronounced for stiffer base layers. For intra-project sensitivity, a linear relationship is again observed, consistent with the trends seen in previous cases. The degree of sensitivity increases with stiffer base layers. Notably, the resulting CoV of pavement deflection can reach up to 20 %, which is higher than the corresponding values observed for $h_{surface}$. This suggests that uncertainties in h_{base} have a more pronounced impact on the statistical variability of pavement deflection compared to the uncertainties in $h_{surface}$.

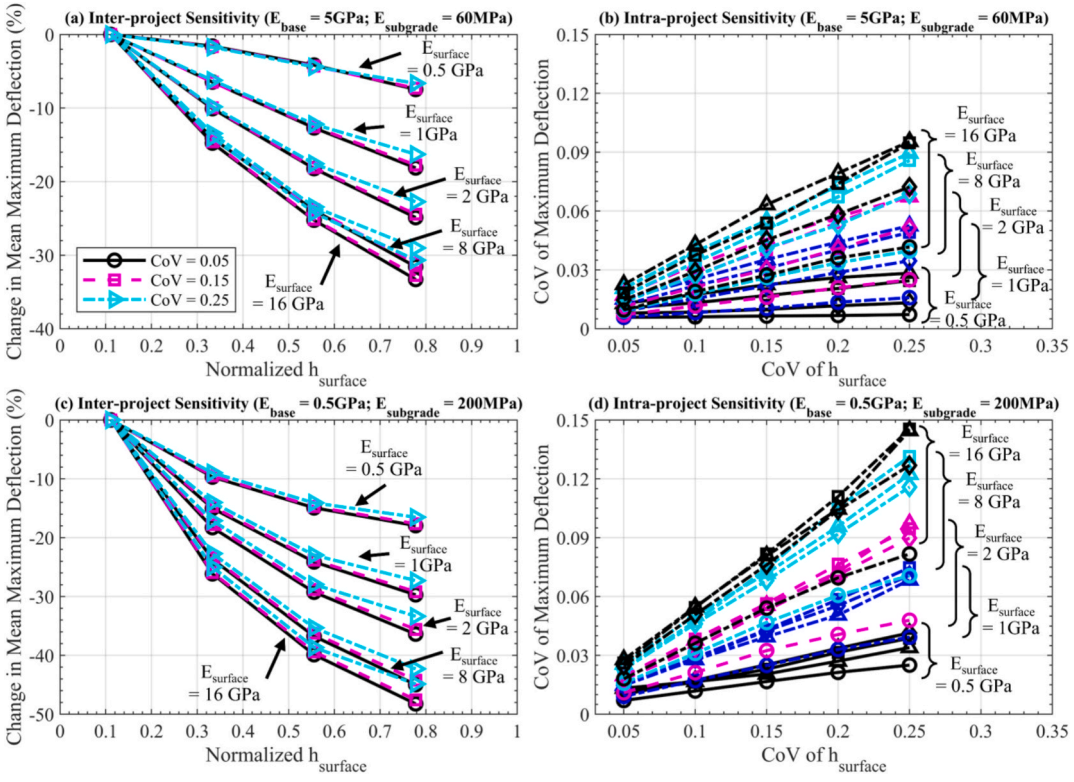

Fig. 9. Results of Case 4 of the probabilistic sensitivity analysis. The different lines shown in subplot (b) and (d) within each $E_{surface}$ group correspond to cases with different mean $h_{surface}$ values.

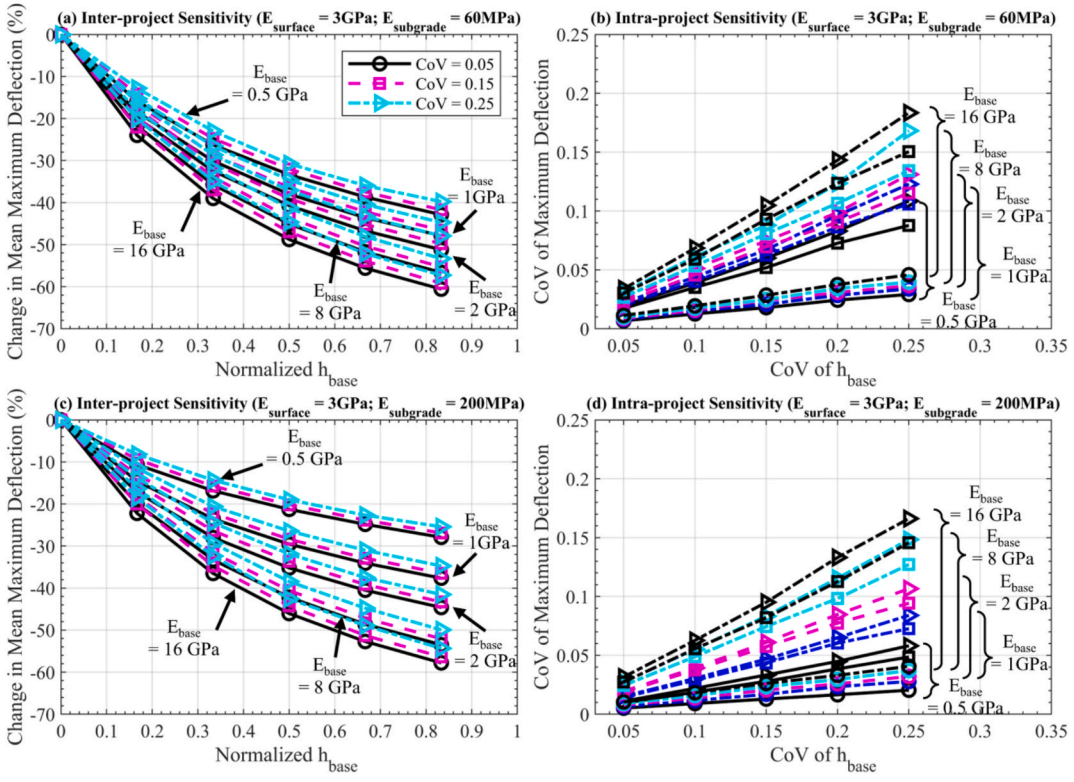

Fig. 10. Results of Case 5 of the probabilistic sensitivity analysis. The different lines shown in subplot (b) and (d) within each E_{base} group correspond to cases with different mean h_{base} values.

Implications on parameter inference

The sensitivity of input parameters has critical implications for parameter inference because it directly influences the identifiability and accuracy of inferred values. Specifically, parameter inference is most effective for parameters to which the system response is sensitive. For parameters exhibiting low sensitivity, multiple parameter values can yield similar system responses, resulting in non-uniqueness in parameter inference. This challenge is particularly significant for deterministic parameter inference techniques such as the residual minimization technique, which provides a single set of inferred parameters by minimizing the difference between simulated and measured system responses. For insensitive parameters, this inferred value may not represent the true solution, as many other parameter combinations could produce similar residuals. Moreover, measurement uncertainties compound this challenge.

Fig. 11 summarizes the average degree of sensitivity across all parameters evaluated in Figs. 6 to 10. For inter-project variability, pavement deflection is found to be most sensitive to $E_{subgrade}$, followed by E_{base} and $E_{surface}$. This ranking implies that TSD measurements are most effective for inferring $E_{subgrade}$ and least effective for $E_{surface}$. In addition, the results suggest that parameter inference is generally more effective for softer pavement systems than for stiffer systems, due to the higher sensitivity of deflection to changes in these parameters in softer layers. In terms of intra-project sensitivity, the very low CoV of deflection associated with $E_{surface}$ and E_{base} indicates that it can be challenging to infer their statistical variability using TSD measurements. In contrast, the statistical variability of $E_{subgrade}$ can be more reasonably inferred using TSD measurements, owing to the stronger sensitivity observed. For geometric parameters, the sensitivity results suggest that TSD measurements are more effective for inferring h_{base} than $h_{surface}$. Furthermore, while the inference of the statistical variability of $h_{surface}$ and h_{base} is moderately feasible, it is still more promising than inferring the variability of $E_{surface}$ and E_{base}.

Bayesian Updating of TSD Data

In this section, Bayesian updating is implemented using simulated TSD measurements to infer both pavement modulus and layer thickness. As outlined in Table 5, two test cases are considered in the present study. In test case 1, TSD measurements are utilized to infer the modulus of all three pavement layers. In test case 2, TSD measurements are used to infer the thickness of the surface and base layers. The results of both test cases are discussed in detail and compared with those obtained with the conventional deterministic residual minimization technique to highlight the advantages associated with Bayesian updating.

Table 5
Prior knowledge of material parameters.

	Parameters	Mean	CoV
Test case 1	$E_{surface}$ (MPa)	3500	0.4
	E_{base} (MPa)	5500	0.4
	$E_{subgrade}$ (MPa)	70	0.4
Test case 2	$h_{surface}$ (m)	0.15	0.3
	h_{base} (m)	0.3	0.3

A major advantage associated with using simulated TSD measurements in the present study is the availability of ground truth parameters—i.e., known material properties and layer thicknesses. This enables parameter inference to be performed in a controlled environment, allowing for an effective validation of the employed parameter inference techniques. Most importantly, with known ground truth, the results can be interpreted alongside the sensitivity analysis results presented in Section "Probabilistic simulation of TSD for sensitivity analysis", especially for verifying the several hypothesized implications discussed in Section "Implication on parameter inference".

Generation of simulated TSD measurements

Following the prior knowledge listed in Table 5, a set of parameter values can be randomly sampled from the defined prior distributions and considered as the ground truth. The trained ANN model then takes these values as inputs to generate the corresponding pavement deflection profiles. Two example cases of deflection profiles generated for test case 1 are shown in Fig. 12. Since the quantity and quality of field measurements can significantly affect the reliability of parameter inference, a total of 10 TSD measurement locations are simulated, reflecting a realistic configuration for modern TSD systems. To simulate TSD measurements more realistically, measurement noise is added to the ANN-generated TSD measurements. In the present study, a ± 5 % measurement error is assumed for the TSD system for demonstration purposes. In practice, if a calibrated measurement error is available, it can be readily incorporated into the Bayesian model updating framework. Following the recommendation of Finno & Calvello [43], such a reported measurement error is typically interpreted as corresponding to the 95 % confidence interval of a normal distribution with zero mean, from which the standard deviation can be back-calculated. Independent noise is then sampled and added to the ANN-generated deflection values to obtain the final simulated TSD measurements for subsequent Bayesian updating. Since TSD sensors at different measuring locations operate independently, it is reasonable to assume uncorrelated measurement uncertainties across locations. The final simulated TSD measurements

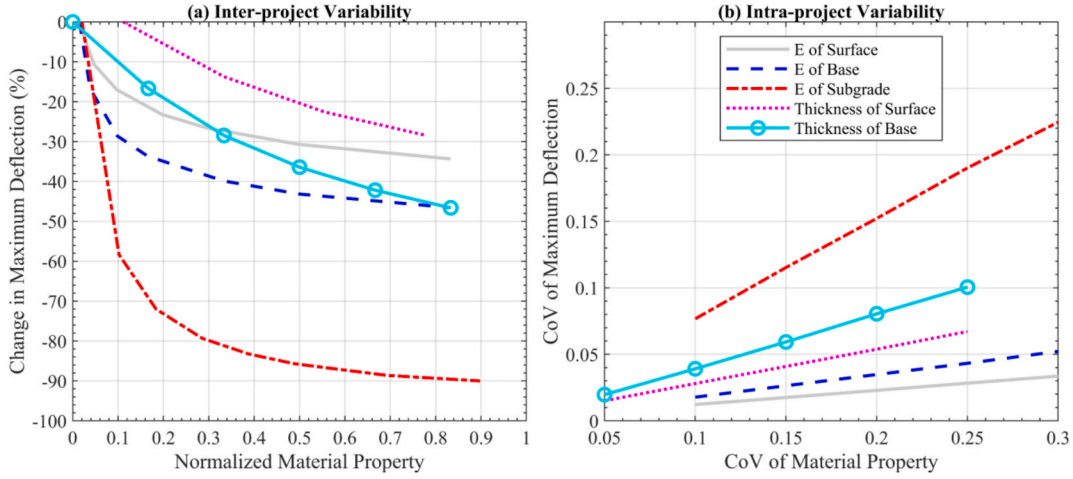

Fig. 11. Average results of the probabilistic sensitivity analyses.

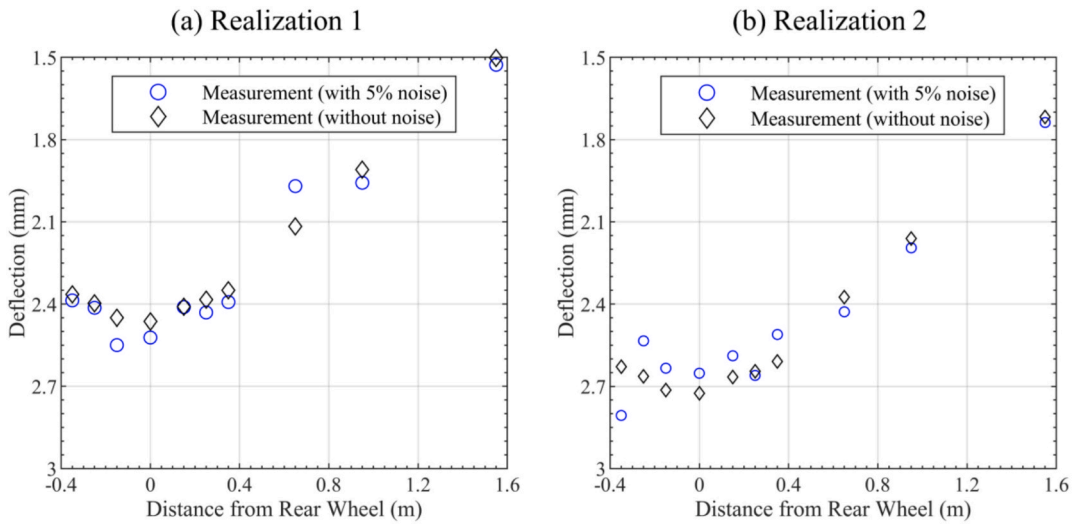

Fig. 12. Examples of simulated TSD data with/without measurement errors for test case 1.

incorporating noise are also shown in Fig. 12 for test case 1.

Bayesian updating

Test case 1

In this section, the simulated TSD measurements shown in Fig. 12(a) are used to statistically infer the three pavement modulus values. As a standard procedure in Bayesian updating using the MCMC-MH algorithm, the length of the Markov chain and the scale factor are first determined. Fig. 13 presents the resulting Markov chain with a total length of 20,000 samples. It is worth highlighting that the trained ANN surrogate model can simulate these samples in approximately 5 min, which contrasts with the 20 days required by the original PaveMove model.

The scale factors are selected using a trial-and-error approach by visually inspecting the behavior of the Markov chain. As shown in Fig. 13, the chain exhibits stable fluctuations around a converged mean and standard deviation without evidence of step-like patterns or drift, indicating appropriate tuning of the scale factors. After discarding the initial 1,000 burn-in samples, the posterior distributions of the three modulus parameters are obtained and shown in Fig. 13. To statistically characterize these distributions, a normal distribution is fitted to the posterior samples, and the corresponding posterior mean and CoV are indicated in the figure.

Fig. 14(a) to (c) compare the posterior distributions with the prior distributions, ground truth parameter values, and the results from the deterministic residual minimization technique. The impact of Bayesian updating varies considerably across the three parameters. For E_{surface}, the posterior CoV is approximately 0.37, only marginally reduced from the prior CoV of 0.4. This indicates the limited effectiveness of Bayesian updating for this parameter. Similarly, the posterior CoV of E_{base} is approximately 26 %, which represents some improvement but remains

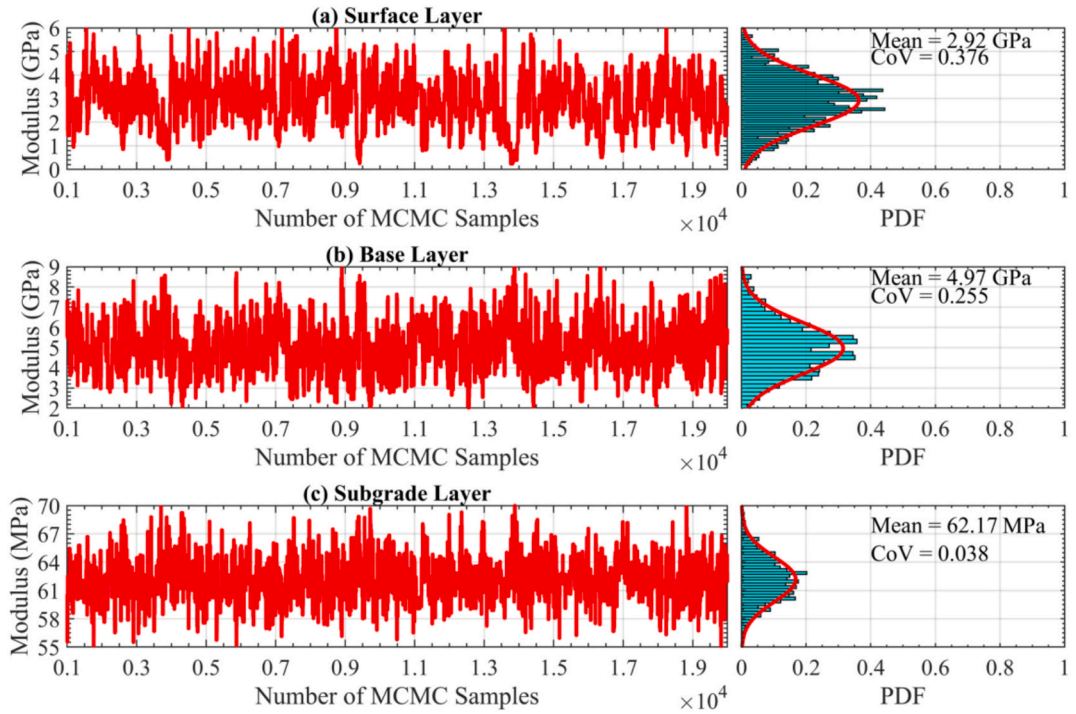

Fig. 13. Convergence of the Markov chain in the MCMC-MH algorithm.

relatively high. In contrast, the effects of Bayesian updating on $E_{subgrade}$ are very significant. The prior CoV of $E_{subgrade}$ is substantially reduced from 40 % to approximately 4 %, showing that Bayesian updating is highly effective for this parameter. Furthermore, across all three parameters, the posterior mean values closely align with the known ground truth, demonstrating the accuracy of the parameter inference. In addition, the residual minimization technique also provides estimates that agree well with the ground truth.

These observations can be interpreted in light of the sensitivity analysis results presented earlier. The limited update in the CoV of $E_{surface}$ and E_{base} is due to the low sensitivity of pavement deflections to these parameters, as indicated in Fig. 11(b). In other words, variations in $E_{surface}$ and E_{base} do not lead to significant changes in deflection, making them hard to infer from TSD measurements. In contrast, deflections are highly sensitive to $E_{subgrade}$, allowing this parameter to be effectively inferred and its uncertainty greatly reduced.

Fig. 15 (a) shows the pavement deflection predictions before and after Bayesian updating. Using only the prior information results in a broad 95 % confidence interval, which, although centered around the simulated TSD measurements, leads to considerable uncertainty that could hinder engineering decision-making. After Bayesian updating, this interval is significantly narrowed and better captures the measurement noise and aligns more closely with the simulated measurements. The residual minimization technique also produces predictions that agree well with the simulated measurements, although it lacks a probabilistic uncertainty estimate.

To assess the consistency of the Bayesian updating, another realization of the simulated TSD measurement is generated and shown in Fig. 12(b). Bayesian updating is then repeated using this new dataset, and the results are shown in Fig. 14 (d) to (f) and 14(b). The findings from this second realization largely mirror those from the first. While the posterior CoVs for $E_{surface}$ and E_{base} remain relatively unchanged, their posterior means still agree well with the ground truth. The most accurate and uncertainty-reduced inference is achieved for $E_{subgrade}$. In addition, the updated 95 % confidence interval in Fig. 15(b) effectively bounds the simulated measurements. In contrast, the residual minimization technique performs poorly in this case for $E_{surface}$ and E_{base}, with large discrepancies observed, although its predictions still align with the simulated measurements. Further discussions on these aspects are provided in Section "Discussion and limitations".

Test case 2

In test case 2, simulated TSD measurements are used to update $h_{surface}$ and h_{base}. Fig. 16(a) shows the realization of the simulated TSD measurements used in this test case. The Markov chain is set to 20,000 samples, and the scale factors are adjusted to ensure the stability of the Markov chain. All other analysis procedures are identical to those described in test case 1.

Fig. 17 shows the results of parameter inference for $h_{surface}$ and h_{base}. It is observed that the posterior CoV of $h_{surface}$ is not effectively reduced by the Bayesian updating, indicating the limited effectiveness of the TSD measurements in improving knowledge of this parameter. In contrast, the posterior CoV of h_{base} exhibits a marked reduction compared to the corresponding prior knowledge, suggesting improved parameter estimation. This difference can also be explained by the sensitivity results shown in Fig. 11. The higher inter-project and intra-project sensitivities

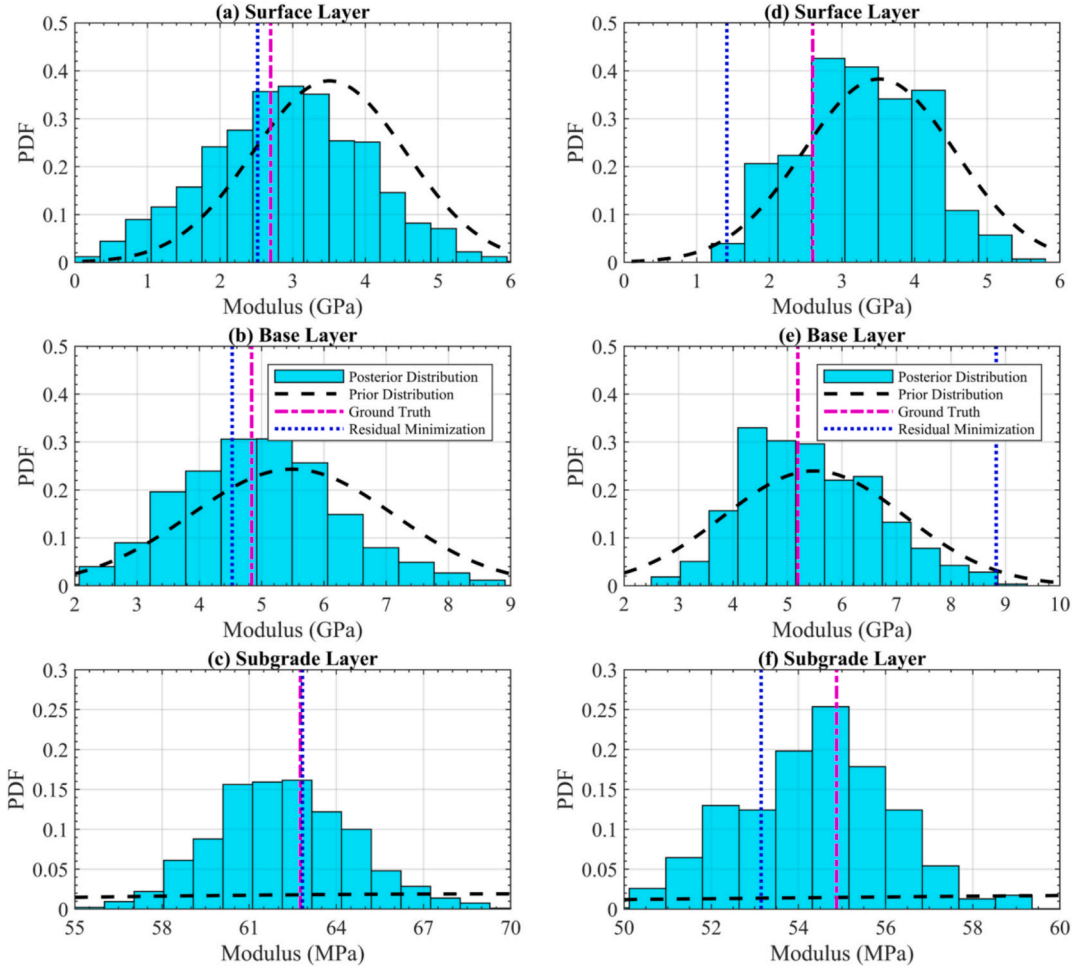

Fig. 14. Comparison of the posterior distributions of the three modulus parameters.

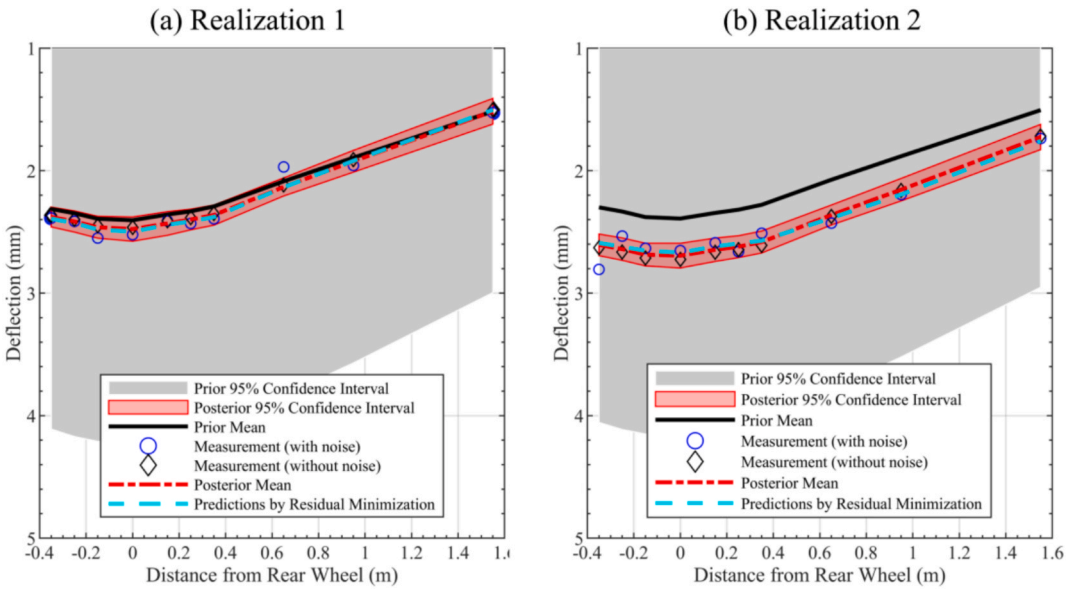

Fig. 15. Pavement deflection predictions before and after Bayesian updating.

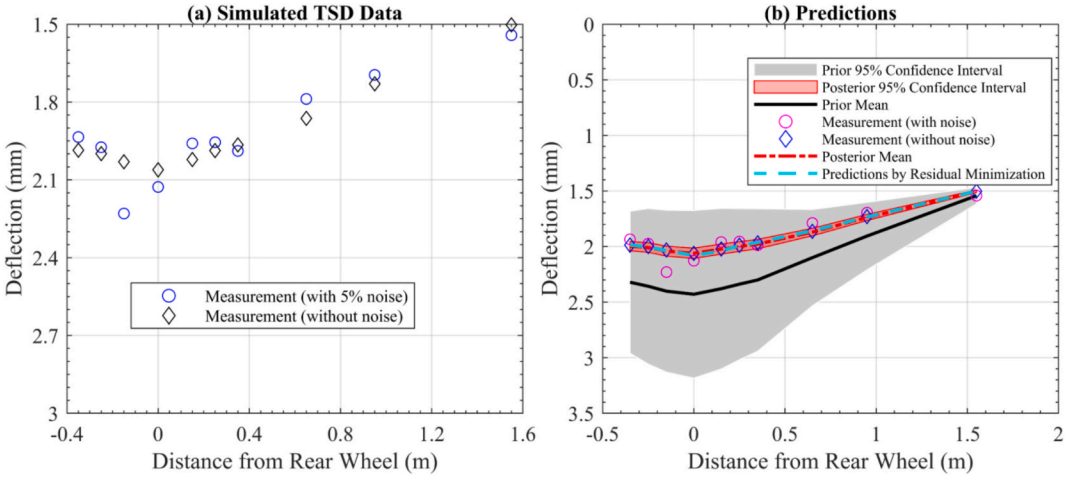

Fig. 16. Simulated TSD measurements and the corresponding predictions in test case 2.

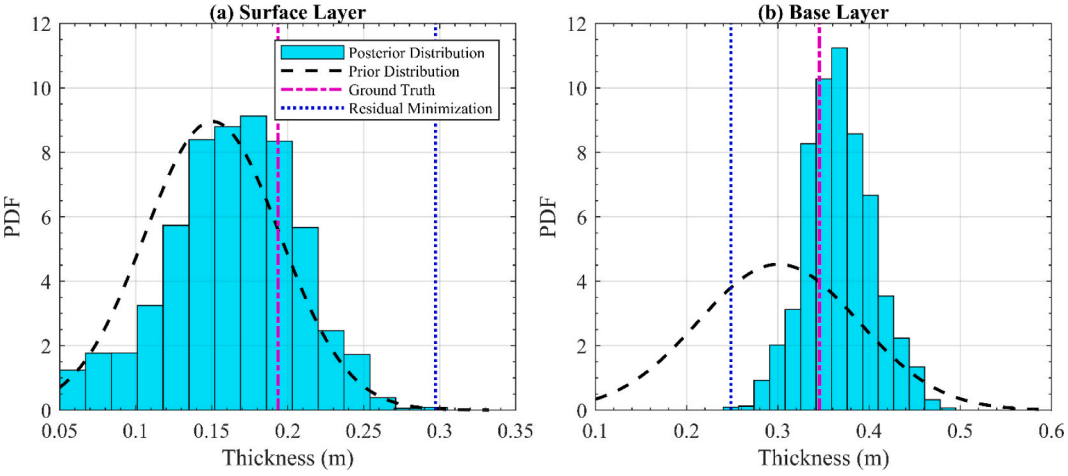

Fig. 17. Results of the parameter inference in test case 2.

associated with h_{base} suggest that TSD measurements are more effective in distinguishing different h_{base} values than $h_{surface}$ values. As a result, the uncertainty reduction is more pronounced for h_{base}. Moreover, the posterior means of both $h_{surface}$ and h_{base} show good agreement with their ground truth values, which demonstrates that Bayesian updating with TSD measurements is reasonably effective in capturing the average parameter values. As a result, the model predictions and their associated 95 % confidence intervals agree well with the simulated TSD measurements. In contrast, for this particular realization, the residual minimization technique fails to infer reasonable values for $h_{surface}$ and h_{base}. However, as shown in Fig. 16(b), the resulting predictions still align well with the simulated measurements. This contrast will be further discussed in the following section.

Discussions and limitations

Consistency in parameter inference

One key benefit of using simulated measurements is the ability to perform repeated analyses for investigating the consistency of different parameter inference techniques. Following the procedures outlined in Section "Bayesian updating of TSD data", a total of 50 repeated analyses are performed. Each analysis involves a different set of randomly generated ground truth parameter values and simulated measurement errors. As a result, for each parameter, 50 corresponding posterior distributions are obtained. Examining these distributions enables a comprehensive evaluation of the consistency and reliability of the parameter inference technique.

Fig. 18 compares the posterior distributions from these 50 repeated analyses with the corresponding ground truth values for the three modulus parameters. The red circles represent the posterior mean values, while the shaded regions represent the 95 % confidence intervals of the posterior distributions. For comparison, the residual minimization technique is also applied to the same 50 repeated analyses. It is observed that the posterior means generally agree well with the ground truth across the 50 repeated analyses, and the ground truth values largely fall within the shaded regions. However, the errors are larger for $E_{surface}$ and E_{base} compared to $E_{subgrade}$. This observation aligns with the sensitivity analysis shown in Fig. 11(a), where the degree of sensitivity for $E_{surface}$ and E_{base} is lower than that for $E_{subgrade}$. A lower degree of sensitivity indicates that multiple $E_{surface}$ and E_{base} can yield similar pavement deflections, making them harder to distinguish accurately using TSD measurements. In contrast, $E_{subgrade}$ displays much greater sensitivity, enabling more accurate posterior estimates. In addition, the posterior CoVs for $E_{surface}$ and E_{base} remain higher than those for $E_{subgrade}$ across the 50 analyses. This trend also matches the intra-project sensitivity findings presented in Fig. 11(b).

On the other hand, the consistency in the residual minimization technique is significantly lower. For $E_{surface}$ and E_{base}, the inferred values from the 50 repeated analyses show considerable scatter across the parameter space, with several results falling outside the 95 % confidence interval of the Bayesian posterior distributions. However, for $E_{subgrade}$, the performance of the residual minimization technique is much more stable and comparable to that of Bayesian updating. Again, these findings are consistent with the relative sensitivities shown in Fig. 11(a): the scatter is largest for $E_{surface}$ and smallest for $E_{subgrade}$, which directly corresponds to their sensitivity levels.

There are two primary reasons why the residual minimization technique produces more scattered results than Bayesian updating. First, Bayesian updating explicitly incorporates prior knowledge through probability distributions, which assigns varying likelihoods to different parameter values. This results in lower probabilities for extreme values. In contrast, residual minimization typically treats prior knowledge as hard bounds for the parameter search, which effectively assigns equal probability across the entire parameter space. Second, Bayesian updating explicitly accounts for measurement uncertainties in the likelihood function. In contrast, residual minimization considers these uncertainties only indirectly—as weights in the objective function of the optimization algorithm. Therefore, residual minimization is more vulnerable to being skewed by measurement errors, resulting in the wide scatter shown in Fig. 18. These two factors collectively hinder the residual minimization technique in accurately inferring $E_{surface}$ and E_{base}, particularly given their moderate levels of sensitivity.

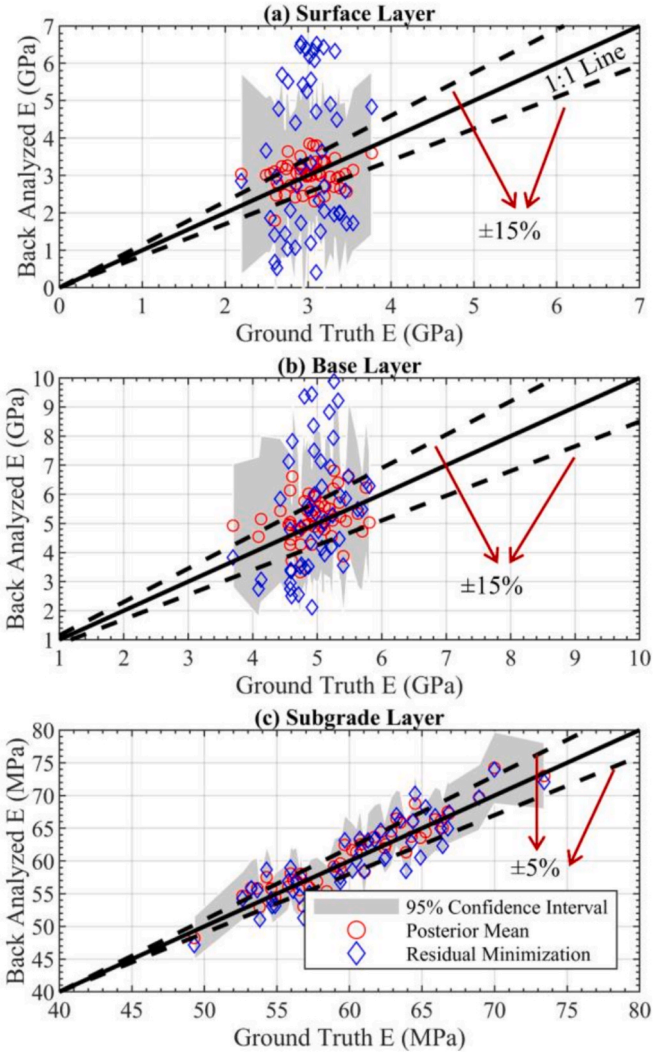

Fig. 18. Consistency of parameter inference techniques in test case 1.

Fig. 19 shows the results of test case 2 based on 50 repeated analyses. While the posterior mean values for both $h_{surface}$ and h_{base} generally align with the ground truth, the 95 % confidence interval for $h_{surface}$ remains consistently wide. In contrast, the confidence interval for h_{base} is consistently narrower, which reflects improved certainty. Similar to the modulus parameters, the residual minimization technique performs inconsistently across repeated analyses, with numerous instances showing significant discrepancies from the ground truth. However, the estimates of h_{base} are comparatively more consistent than those for $h_{surface}$. All these observations are in agreement with the results shown in Fig. 17 and can be similarly explained using the arguments presented earlier in this section.

Extrapolation to other pavement conditions

As observed in Section "Bayesian updating of TSD data", although the parameter values identified by the residual minimization technique may not be correct, they can still produce deflections that match the

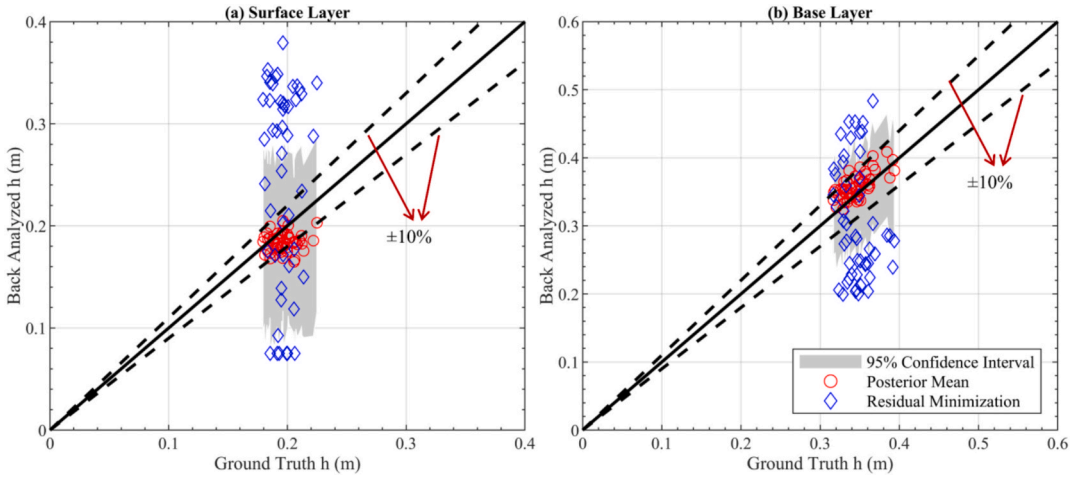

Fig. 19. Consistency of parameter inference techniques in test case 2.

simulated TSD measurements. This outcome is not unexpected because residual minimization explicitly targets minimizing the absolute differences between model predictions and measurements. However, due to the presence of measurement error, the inferred parameter values may be skewed relative to their true values, leading to a false sense of accuracy in the model predictions. As a result, the close agreement between predicted and measured deflections can be misleading and may conceal the fact that the underlying parameter values are incorrect.

In many practical applications, pavement parameters inferred from TSD measurements are often used to simulate pavement responses under different loading or structural conditions. For example, engineers may use the inferred parameters to predict deflections under varying truck speeds, loads, or layer thicknesses. To investigate how well the inferred parameters generalize to different pavement configurations, an extrapolation study is conducted. Three sets of simulated TSD measurements are generated following the setup used in test case 1. Parameter inference is then performed to obtain the posterior distributions of $E_{surface}$, E_{base}, and $E_{subgrade}$. These posterior distributions are subsequently used as inputs to simulate deflections under TSD loading in a new pavement system, which is characterized by a $h_{surface}$ of 0.25 m, a h_{base} of 0.3 m, a truck speed of 50 km/h, and a truck load of 60 kN.

Fig. 20 shows the results of this extrapolation exercise. Subplots (a) to (c) show the original simulated TSD measurements used for parameter inference, along with the corresponding deflection predictions obtained using both Bayesian updating and residual minimization. Both techniques produce deflections that reasonably match the ground truth. Subplots (d) to (e) show the deflection predictions made for the new pavement system using the parameters obtained from each method. The ground truth deflections are also shown for comparison and verification purposes. It is evident that the predictions made with the posterior distributions from Bayesian updating remain reasonable, with the mean predictions closely aligning with the ground truth and the 95 % confidence interval fully capturing the actual deflections. In contrast, the predictions made with the parameter identified using residual minimization show large discrepancies from the ground truth, indicating that incorrect parameter values were identified using TSD measurements in the original analysis (e.g., Table 6).

To further evaluate the robustness of these results, the extrapolation

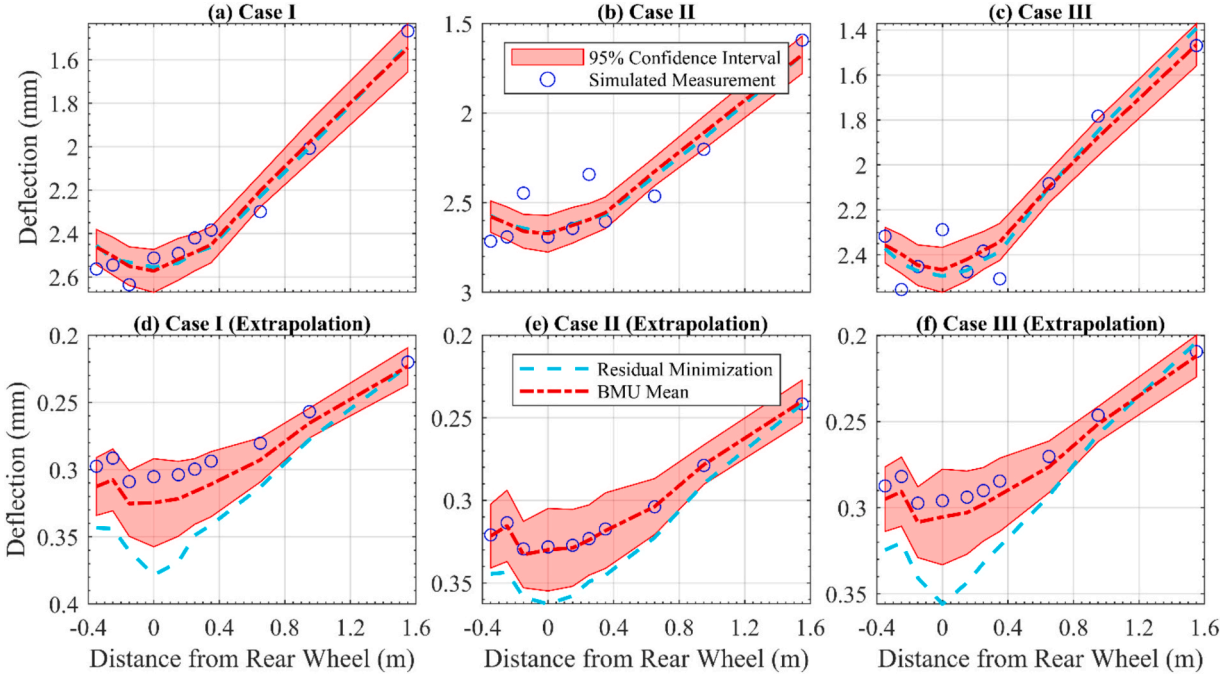

Fig. 20. Demonstration of extrapolation to a different pavement system.

Table 6
Results of parameter identifications.

		Case I	Case II	Case III
$E_{surface}$ (GPa)	Ground truth	3.09	2.71	2.62
	Bayesian updating (posterior mean)	2.53	2.96	2.82
	Residual minimization	**0.42**	**1.52**	**0.53**
E_{base} (GPa)	Ground truth	4.27	5.32	4.73
	Bayesian updating (posterior mean)	4.87	5.08	4.28
	Residual minimization	**7.07**	**7.54**	**4.85**
$E_{subgrade}$ (MPa)	Ground truth	61.8	55.8	65.2
	Bayesian updating (posterior mean)	61.2	56.2	64.4
	Residual minimization	61.6	56.1	68.2

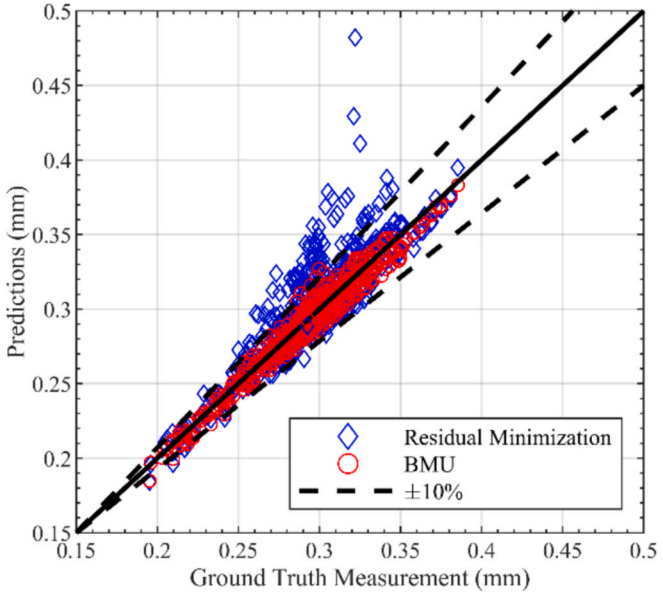

Fig. 21. Comparison of extrapolated pavement deflections for 50 repeated analyses.

exercise is repeated 50 times using different sets of ground truth parameters. Fig. 21 summarizes the comparison between the ground truth deflections and those predicted using the inferred parameter for all 50 analyses. The extrapolation results from Bayesian updating largely agree with the ground truth deflections, as evidenced by the clustering of red scatter points along the 1:1 diagonal line. In contrast, the results from residual minimization show greater variability. While some predictions are reasonable, many deviate significantly from the 1:1 line, confirming that the residual minimization technique identifies inaccurate parameter values that lead to poor extrapolation performance. Based on Fig. 21, it is demonstrated that Bayesian updating, which explicitly incorporates both prior distributions and measurement uncertainties, is more effective in identifying accurate parameter values that can be more reliably used for extrapolation across varying pavement conditions, in comparison to the residual minimization technique.

Practical implications

Since TSD differs fundamentally from FWD in its loading mechanisms, converting TSD data to FWD-equivalent data lacks a solid mechanistic foundation. From a practical perspective, the adoption of TSD, being a more complex and costly technology, requires careful assessment of its cost-effectiveness and technological readiness. In the UK, NDT techniques are adopted to assess road structural strength, and the results are used with pavement construction and traffic to determine the Network Structural Condition category for each 100 m section. Although TSD has been available as an NDT technology in the UK for many years, its use in practice remains largely qualitative. The UK road sector has reported inconsistencies between the interpreted results of TSD and FWD, such as the back-calculated material parameters and the Network Structural Condition category, thereby raising concerns about the adoption of TSD in place of FWD in practice. One of the key barriers to its wider quantitative adoption is the absence of accessible and reliable predictive models based on TSD measurements. The provision of the proposed framework in the present study addresses this gap and contributes to enhancing the technological readiness of TSD-based pavement evaluation. The developed PaveMove, which directly simulates TSD, provides a ready-to-use simulation tool. The integration of machine learning significantly improves computational efficiency and allows timely interpretation of large volumes of TSD data—an essential feature given TSD's continuous data collection mode. By enabling faster, real-time analysis within a given test duration and budget (compared to FWD), and eliminating the need for road closures, the framework potentially increases the cost-effectiveness and safety of pavement condition assessments. Ultimately, it offers a viable path toward integrating TSD technology into modern, network-level pavement management systems in a more quantitative, informed, and efficient manner.

Limitations and future work

Future work is encouraged to address some limitations of the present study and explore further opportunities in pavement parameter inference using TSD measurements. First, $E_{surface}$, E_{base}, $E_{subgrade}$, $h_{surface}$, and h_{base} are not simultaneously updated using TSD measurements. This is due to the issue of parameter compensation. For example, a soft but thick surface layer may result in deflections similar to those of a stiff but thin surface layer. When all five parameters are simultaneously considered, such compensatory effects can become more complex and exacerbate the challenge of unique parameter identification. As a result, relying solely on TSD measurements is often insufficient for reliably updating all these parameters together. In practice, additional sources of information such as ground-penetrating radar (GPR) are often used to estimate layer thicknesses. Future studies should explore the integration of TSD measurements with GPR measurements for a more comprehensive and robust probabilistic parameter inference framework.

Second, the study finds that some parameters—$E_{surface}$, E_{base}, $h_{surface}$, and h_{base}—exhibit only a moderate degree of sensitivity with respect to pavement deflections. For these parameters, reasonably accurate prior knowledge (e.g., prior mean values that are not significantly biased) is often required to ensure effective Bayesian updating using TSD measurements. When the prior information for these parameters is poorly estimated, Bayesian updating using TSD measurements may perform inadequately due to the limited sensitivity of deflections to changes in these parameters.

Third, the present study considers pavement deflection as the primary output quantity of interest. However, the direct measurement obtained from a TSD device is the deflection slope. While deflections can be converted from slopes through some means [29], focusing directly on deflection slope as the observable quantity in Bayesian updating may provide a more accurate and direct representation of TSD measurements. Future studies are warranted to investigate the use of deflection slope in parameter inference, which may further improve the validity and applicability of Bayesian updating for TSD-based pavement evaluation. Last, the present study assumes all pavement layers are elastic, which may not be fully representative of the various layers. Future studies will directly incorporate viscoelastic behavior to more realistically simulate the surface layer. This is possible using PaveMove's built-in viscoelastic material model. In addition, advanced techniques that correlate viscoelastic to elastic behavior for simplified analysis will also be explored [15,16].

Conclusions

In summary, this paper presents the first end-to-end probabilistic framework for inferring pavement material parameters using TSD measurements. It overcomes three limitations of existing TSD-based parameter inference techniques through a synergistic combination of a physics-based simulator (PaveMove), machine learning surrogates, and Bayesian updating. Rigorous validation using a series of simulated TSD datasets demonstrates improved performance compared to conventional deterministic residual minimization techniques. The specific key conclusions are as follows:

(i) PaveMove effectively simulates mechanical pavement responses under TSD dynamic loading, establishing itself as a new and practical simulation tool for TSD-based pavement structural evaluation.
(ii) A validated machine learning surrogate model is successfully developed to emulate PaveMove across a broad range of pavement material properties. It acts as an effective computational tool to permit real-time probabilistic parameter inference using TSD measurements, which align well with the continuous nature of TSD data acquisition.
(iii) The accuracy of TSD-based parameter inference varies across parameters. Parameter inference using TSD deflections is more reliable for inferring $E_{subgrade}$ than for E_{base} and $E_{surface}$, and for inferring h_{base} than for $h_{surface}$. Compared to deterministic residual minimization, Bayesian updating provides more consistent parameter estimates, particularly for parameters with lower sensitivity, such as E_{base}, $E_{surface}$, and $h_{surface}$. Moreover, its ability to quantify uncertainties explicitly supports the proactive validation and interpretation of inferred parameters. From a practical point of view, Bayesian updating is recommended for TSD-based parameter inference.
(iv) The synergistic combination of the three core components in the proposed methodological framework significantly enhances the technological readiness of TSD-based pavement evaluation. It lays a solid foundation for the broader, quantitative integration of TSD technology into modern, network-level pavement management systems.

CRediT authorship contribution statement

Ze Zhou Wang: Writing – review & editing, Writing – original draft, Methodology, Investigation, Formal analysis, Data curation, Conceptualization. **Zhaojie Sun:** Writing – review & editing, Writing – original draft, Validation, Methodology, Investigation, Conceptualization. **Bachar Hakim:** Supervision, Resources, Project administration. **Buddhima Indraratna:** Supervision, Project administration. **Abir Al-Tabbaa:** Supervision, Project administration, Funding acquisition.

Disclaimer

This study reflects only the author's view and that the Agency and the Commission are not responsible for any use that may be made of the information it contains.

Declaration of competing interest

The authors declare that they have no known competing financial interests or personal relationships that could have appeared to influence the work reported in this paper.

Acknowledgments

This project is funded by the European Union's Horizon 2020 research and innovation program under the Marie Skłodowska-Curie grant agreement No. 101034337.

Data availability

Some or all data, models, or codes that support the findings of this study are available from the corresponding author upon reasonable request.

References

[1] Correia AG, Winter MG, Puppala AJ. A review of sustainable approaches in transport infrastructure geotechnics. Transp Geotech 2016;7:21–8.
[2] Koks EE, Rozenberg J, Zorn C, Tariverdi M, Vousdoukas M, Fraser SA, et al. A global multi-hazard risk analysis of road and railway infrastructure assets. Nat Commun 2019;10(1):2677.
[3] Wang C, Lim MK, Zhang X, Zhao L, Lee PTW. Railway and road infrastructure in the Belt and Road Initiative countries: estimating the impact of transport infrastructure on economic growth. Transp Res A Policy Pract 2020;134:288–307.
[4] Wang ZZ, Goh SH, Koh CG, Smith IF. Comparative study of the effects of three data-interpretation methodologies on the performance of geotechnical back analysis. Int J Numer Anal Meth Geomech 2020;44(15):2093–113.
[5] Gudipudi PP, Underwood BS, Zalghout A. Impact of climate change on pavement structural performance in the United States. Transp Res Part D: Transp Environ 2017;57:172–84.
[6] Pandey P, Hossain MS, Ahmed A. Performance evaluation of modified moisture barrier in mitigating expansive soil associated pavement distresses. Transp Geotech 2021;31:100667.
[7] Zeng W, Wu S, Wen J, Chen Z. The temperature effects in aging index of asphalt during UV aging process. Constr Build Mater 2015;93:1125–31.
[8] Yin F, Arámbula-Mercado E, Epps Martin A, Newcomb D, Tran N. Long-term ageing of asphalt mixtures. Road Mater Pavement Des 2017;18(sup1):2–27.
[9] Zaabar I, Chatti K. Estimating vehicle operating costs caused by pavement surface conditions. Transp Res Rec 2014;2455(1):63–76.
[10] Kobayashi K, Kaito K, Lethanh N. A statistical deterioration forecasting method using hidden Markov model for infrastructure management. Transp Res B Methodol 2012;46(4):544–61.
[11] Marcelino P, de Lurdes Antunes M, Fortunato E, Gomes MC. Machine learning approach for pavement performance prediction. Int J Pavement Eng 2021;22(3):341–54.
[12] Xiao F, Chen X, Cheng J, Yang S, Ma Y. Establishment of probabilistic prediction models for pavement deterioration based on Bayesian neural network. Int J Pavement Eng 2022:1–16.
[13] Mers M, Yang Z, Hsieh YA, Tsai Y. Recurrent neural networks for pavement performance forecasting: review and model performance comparison. Transp Res Rec 2023;2677(1):610–24.
[14] Pasupunuri SK, Thom N, Li L. Roughness prediction of jointed plain concrete pavement using physics informed neural networks. Transp Res Rec 2024;2678(11):1733–46.
[15] Chen K, Torbaghan ME, Thom N, Faramarzi A. Physics-guided neural network for predicting international roughness index on flexible pavements considering accuracy, uncertainty and stability. Eng Appl Artif Intel 2025;142:109922.
[16] Chen Z, Tong X, Cheng H, Sun L. Conversions of viscoelastic deflections of asphalt pavement under TSD load to elastic ones for pavement condition assessments. Road Mater Pavement Des 2025;26(1):158–80.
[17] Duong NS, Blanc J, Hornych P, Bouveret B, Carroget J, Le Feuvre Y. Continuous strain monitoring of an instrumented pavement section. Int J Pavement Eng 2019;20(12):1435–50.
[18] Liu Z, Gu X, Wu C, Ren H, Zhou Z, Tang S. Studies on the validity of strain sensors for pavement monitoring: a case study for a fiber Bragg grating sensor and resistive sensor. Constr Build Mater 2022;321:126085.
[19] Wang J, Han Y, Cao Z, Xu X, Zhang J, Xiao F. Applications of optical fiber sensor in pavement Engineering: a review. Constr Build Mater 2023;400:132713.
[20] Shen K, Wang H. Prediction of critical strains of flexible pavement from traffic speed deflectometer measurements. Constr Build Mater 2024;411:134770.
[21] Nega A, Nikraz H, Al-Qadi IL. Dynamic analysis of falling weight deflectometer. J Traffic Transport Eng (Engl Ed) 2016;3(5):427–37.
[22] Coletti K, Romeo RC, Davis RB. Bayesian backcalculation of pavement properties using parallel transitional Markov chain Monte Carlo. Comput Aided Civ Inf Eng 2024;39(13):1911–27.
[23] Li C, Gao G, Shen P, Wang Y, Wang Y. Deep learning-based inversion of soil and rock compaction density utilizing Falling Weight Deflectometer (FWD) and Surface Waves. Transp Geotech 2024;49:101421.
[24] Zihan ZU, Elseifi MA, Icenogle P, Gaspard K, Zhang Z. Mechanistic-based approach to utilize traffic speed deflectometer measurements in backcalculation analysis. Transp Res Rec 2020;2674(5):208–22.
[25] Katicha S, Flintsch G, Diefenderfer B. Ten years of traffic speed deflectometer research in the United States: a review. Transp Res Rec 2022;2676(12):152–65.
[26] Zhang M, Gong H, Jia X, Jiang X, Feng N, Huang B. Determining pavement structural number with traffic speed deflectometer measurements. Transp Geotech 2022;35:100774.
[27] Zhang M, Fu G, Ma Y, Xiao R, Huang B. Speed and temperature superposition on traffic speed deflectometer measurements. Transp Geotech 2023;40:100990.

[28] Krarup, J., Rasmussen, S., Larsen, L. A., & Hjorth, P. G. (2006). Output from the greenwood traffic speed deflectometer.
[29] Tong X, Chen Z, Cheng H, Sun L, Li Y, Min X, et al. Improved deflection calculation methods for traffic speed deflectometers for asphalt pavement condition assessments. Int J Pavement Eng 2025;26(1):2498080.
[30] Xiao F, Xiang Q, Hou X, Amirkhanian SN. Utilization of traffic speed deflectometer for pavement structural evaluations. Measurement 2021;178:109326.
[31] Nasimifar S. 3D-move simulation of TSDDs for pavement characterizations. Reno: University of Nevada; 2015.
[32] Nasimifar M, Thyagarajan S, Sivaneswaran N. Backcalculation of flexible pavement layer moduli from traffic speed deflectometer data. Transp Res Rec 2017;2641(1):66–74.
[33] Sun Z, Kasbergen C, van Dalen KN, Anupam K, Skarpas A, Erkens SM. A parameter identification technique for traffic speed deflectometer tests of pavements. Road Mater Pavement Des 2023;24(4):1065–87.
[34] Fathi S, Mehravar M, Rahman M. Development of FWD based hybrid back-analysis technique for railway track condition assessment. Transp Geotech 2023;38:100894.
[35] Mabrouk GM, Elbagalati OS, Dessouky S, Fuentes L, Walubita LF. 3D-finite element pavement structural model for using with traffic speed deflectometers. Int J Pavement Eng 2022;23(12):4065–79.
[36] Sun Z, Kasbergen C, Skarpas A, van Dalen KN, Anupam K, Erkens SM. A nonlinear spectral element model for the simulation of traffic speed deflectometer tests of asphalt pavements. Int J Pavement Eng 2022;23(4):1186–97.
[37] Hamidi A, Hoff I, Mork H. Elastic and viscoelastic back-calculation of pavement layers' moduli using data obtained from traffic speed deflection devices. Constr Build Mater 2024;447:138035.
[38] Liu P, Xing Q, Dong Y, Wang D, Oeser M, Yuan S. Application of finite layer method in pavement structural analysis. Appl Sci 2017;7(6):611.
[39] Sun Z, Kasbergen C, Skarpas A, Anupam K, van Dalen KN, Erkens SM. Dynamic analysis of layered systems under a moving harmonic rectangular load based on the spectral element method. Int J Solids Struct 2019;180:45–61.
[40] Nielsen CP. Visco-elastic back-calculation of traffic speed deflectometer measurements. Transp Res Rec 2019;2673(12):439–48.
[41] Jiang SH, Hu HP, Wang ZZ. Improved Bayesian model updating of geomaterial parameters for slope reliability assessment considering spatial variability. Struct Saf 2025;112:102536.
[42] Cheung SH, Beck JL. Bayesian model updating using hybrid Monte Carlo simulation with application to structural dynamic models with many uncertain parameters. J Eng Mech 2009;135(4):243–55.
[43] Finno RJ, Calvello M. Supported excavations: observational method and inverse modelling. J Geotech Geoenviron Eng 2005;131(7):826–36.
[44] Qi XH, Zhou WH. An efficient probabilistic back-analysis method for braced excavations using wall deflection data at multiple points. Comput Geotech 2017;85:186–98.
[45] Corley-Lay J, Morrison CS. Layer thickness variability for flexible pavements in North Carolina. Transp Res Rec 2001;1778(1):107–12.
[46] Zhong XG, Zeng X, Rose JG. Shear modulus and damping ratio of rubber-modified asphalt mixes and unsaturated subgrade soils. J Mater Civ Eng 2002;14(6):496–502.
[47] Kuo CM, Tsai TY. Significance of subgrade damping on structural evaluation of pavements. Road Mater Pavement Des 2014;15(2):455–64.
[48] Fernandes FM, Fernandes A, Pais J. Assessment of the density and moisture content of asphalt mixtures of road pavements. Constr Build Mater 2017;154:1216–25.
[49] Dalla Valle P, Thom N. Improvement to method of equivalent thicknesses (MET) for calculation of critical strains for flexible pavements. Int J Pavement Eng 2018;19(12):1053–60.
[50] Valle, P. D., & Thom, N. (2020). c. *International Journal of Pavement Engineering, 21* (7), 930-938.
[51] Li M, Dai Q, Su P, You Z, Ma Y. Surface layer modulus prediction of asphalt pavement based on LTPP database and machine learning for Mechanical-Empirical rehabilitation design applications. Constr Build Mater 2022;344:128303.